CDF/ANAL/TOP/CDFR/11055
Version 5.00
January 27, 2014

Top Quark Mass Measurement in the Dilepton Channel Using the Full CDF Data Set

Julian Budagov[1], Vladimir Glagolev[1], Igor Suslov[1], George Velev[2]

Abstract

We present a measurement of the top-quark mass in the dilepton channel using the full CDF Run II data set, corresponding to an integrated luminosity of 9.1 fb^{-1}. After applying the selection cuts, 520 events are obtained. We analyze these events using two initial variables, which are sensitive to different kinematic properties of the $t\bar{t}$ system. The first variable is the reconstructed top quark mass obtained with a kinematic fit of the dilepton events. Our second variable is calculated in a way that it is insensitive to the jet energy scale (JES). This variable allows us to reduce the systematic error due to the JES uncertainty. Applying a template analysis, we determine the top-quark mass using a variable defined as a weighted sum of the upper two variables. For the this analysis, the templates are built from simulated $t\bar{t}$ and background events and parameterized in order to provide smooth probability distribution functions (p.d.f.'s). A likelihood fit of the data to a weighted sum of signal and background p.d.f.'s returns the top-quark mass of $170.80 \pm 1.83(\text{stat.}) \pm 2.69(\text{syst.})$ GeV/c^2.

[1]JINR, Dubna

[2]Fermilab

Contents

1 Introduction

The analysis presented in this note updates the CDF result on top mass in the dilepton channel using the full CDF Run II data set of 9.1 fb^{-1}. The updated result is intended to be used in the Tevatron and world top-quark mass combination [1]. The last CDF mass result in this channel [2] was obtained with a data set corresponding to 5.6 fb^{-1}. Currently, we have more than 3 fb^{-1} of additional data that never been analyzed in purpose of the top-quark mass determination.

With increasing of the data, the top-mass analysis in the dilepton channel has new distinctive feature: statistical error is not anymore the leading uncertainty in the measurement. The main limitation arises from the systematic error, which is dominated by the jet energy scale (JES) uncertainty. In contrast to l+jets and all-hadronic channels, in the dilepton events, there are no quarks originated from W boson decay and as a consequence there is no a dijet mass constrain, which permits a precise calibration of the calorimeter JES. This fact requires to direct our effort towards searches of new possibilities for reduction of the systematic uncertainty of the top mass due to the uncertainties in JES.

DØ collaboration performed an analysis that attempts to carry over the JES value obtained in the l+jets top-mass analysis to the jets in dilepton sample [3]. We don't exploit this idea due to the fact that our result would depend on the l+jets top mass. By construction in the l+jets analysis, the JES calibration extracted from the l+jets data fit, would have a large correlation with the top mass and if we use this calibration in the dilepton events we implicitly impose that the top masses in both samples are the same.

In this analysis, we optimize the combine uncertainty that includes two main parts: statistical and JES uncertainties. Practically, we take two initial variables with different properties. First variable is reconstructed mass from the kinematic fit of the dilepton events. We use this variable due to the fact that it is the most sensitive to the value of the top mass. In contrast to the reconstructed mass, our second variable is the most sensitive to top mass that we can build without using any jet energy information in the events. Therefore, this variable is insensitive to JES but still has some sensitive to the top mass. Finally, we define the "hybrid" variable for template analysis using a weighted sum of these two variables. The weight is chosen by requirement of minimal expected $stat \oplus JES$ uncertainty. The method allows us to reduce the expected $stat \oplus JES$ uncertainty by 12% in comparison to the case if we would use only the reconstructed mass for the analysis.

2 Data Sample and Event Selection

Our top quark mass analysis uses the full RUN II data set collected by CDF and corresponds to a total integrated luminosity of 9.1 fb^{-1}. The events were collected with an inclusive lepton triggers that require an electron with $E_T > 18$ GeV (or a muon with $P_T > 18$ GeV/c) in the central region of the detector. The mass sample was obtained from the data set by applying the "DIL selection criteria" developed for the CDF $t\bar{t}$ cross section measurement in the dilepton channel [4]. In our analysis, we have introduced additional cuts to improve the MC modeling and to reduce the background contributions.

We list the major selection requirements and refer for details to the x-section note [4]. We started our selection with two high-E_T leptons of opposite charge, one of which must be

isolated. For electrons, we require $E_T > 20$ GeV while for the muons - $P_T > 20$ GeV/c. The missing transverse energy,indicating the presence of neutrinos, must be $\not\!\!E_T > 25$ GeV. A Z-veto cut eliminates ee and $\mu\mu$ events with insufficient missing E_T significance and with dilepton invariant mass in the Z-window. An L-shape cut, designed to reject $Z \to \tau\tau$ and events with mis-measured $\not\!\!E_T$, requires the angle between $\vec{\not\!\!E}_T$ and the nearest jet to be $\Delta\phi$ >20° if $\not\!\!E_T < 50$ GeV. Two (or more) jets with corrected $E_T > 15$ GeV and $|\eta| < 2.5$ are also required. The transverse energy sum (H_T) has to be more than 200 GeV. Additionally, the dilepton invariant mass has to be larger than 5 GeV.

The cuts, specific to this analysis, are presented below. We require the minimal cone radius between any lepton and any jet in the events, $\Delta R_{lj} = \sqrt{\Delta\eta_{lj}^2 + \Delta\phi_{lj}^2}$, to be more than 0.2. This cut allows us to reduce significantly background from events with fake lepton (see Figure 1). Also we eliminate events with reconstructed top mass (M_t^{reco}, see section 4) more than 250 GeV. We introduce this requirement to cut on the tail of M_t^{reco} distribution that contains mainly background events. (S/B ratio in the region $M_t^{reco} > 250$ GeV is estimated to be 1:3). Using the M_t^{reco}-cut, we reject 11 events from our sample. Additionally, we strengthen the dilepton invariant mass cut requiring the dilepton mass to be greater than 10 GeV. This cut rejects events from the physics processes, which our MC do not model well.

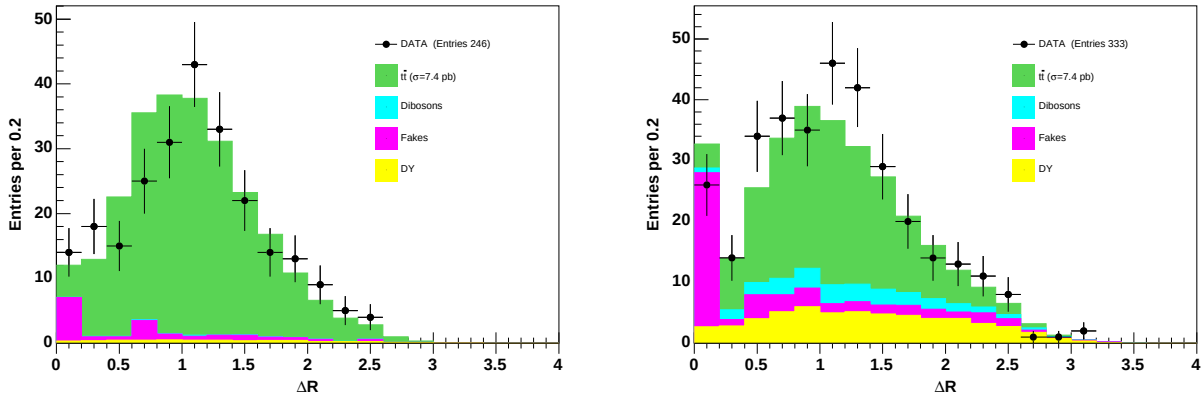

Figure 1: Distribution of the minimal cone radius (ΔR_{lj}) between any lepton and any jet in b-tagged (left) and non-tagged (right) subsamples obtained after DIL selection requirements. Data are overlaid with the MC prediction for the signal and background.

In total, we have selected 520 dilepton candidate events. The same cuts are applied to the Monte Carlo events generated for the signal or background processes. To increase the sensitivity of our measurement to the top-quark mass, we separate our signal sample to two mutually exclusive sub-samples with different S/B ratio: b-tagged and non-tagged events. First sub-sample contains events with at least one tight SecVtx b-tagged jet. Non-tagged sub-sample contains events with no tight SecVtx b-tagged jet, and events, for which we do not have pixel information from the silicon detector.

Our estimation of the data sample composition is based on the result presented in the cross section analysis [4]. We correct for the efficiencies of our additional cuts. These efficiencies

are presented in Table 1. Tables 2 and 3 shows the summary of expected contributions and observed events for the b-tagged and non-tagged samples.

Process	Efficiency		
	Pretag	Tagged	Non-tagged
$t\bar{t}$	0.970 ± 0.001	0.971 ± 0.001	0.969 ± 0.001
Fakes	0.466 ± 0.043	0.550 ± 0.091	0.440 ± 0.049
WW	0.943 ± 0.005	0.973 ± 0.019	0.942 ± 0.049
WZ	0.934 ± 0.008	0.892 ± 0.062	0.935 ± 0.008
ZZ	0.869 ± 0.014	0.693 ± 0.113	0.884 ± 0.013
$Z/\gamma^* \to ee$ (in Z-window)	0.861 ± 0.027	-	-
$Z/\gamma^* \to \mu\mu$ (in Z-window)	0.923 ± 0.022	-	-
$Z/\gamma^* \to ee$ (out Z-window)	0.866 ± 0.014	-	-
$Z/\gamma^* \to \mu\mu$ (out Z-window)	0.844 ± 0.014	-	-
$Z/\gamma^* \to \tau\tau$	0.931 ± 0.013	-	-
$Z/\gamma^* \to \mu\mu$ (as $e\mu$)	0.899 ± 0.019	-	-
DY/Z+LF	-	0.845±0.014	-
DY/Z+HF	-	0.838±0.019	-

Table 1: Total efficiency of the additional cuts (ΔR_{lj} >0.2, $M_t^{reco} < 250$GeV and M_{ll} >10GeV) for the signal and background processes. Values for pre-tagged, tight SecVtx b-tagged and non-tagged samples are presented.

3 Signal and Background Processes Modeling

In this analysis, we use a set of Monte Carlo samples generated by Top group with the Gen6 MC Production software [5]. Our modeling of the signal events is based on samples generated by Pythia v6.216 MC for top quark masses ranging from 160 GeV/c^2 to 185 GeV/c^2 with 1 GeV/c^2 steps. In many studies, we use as nominal the Pythia MC sample, which corresponds to M_{top} =172.5 GeV/c^2. $t\bar{t}$ samples obtained with other MC generators are used for studies of the systematic uncertainties and they are described in Section 6. To model the WW, WZ and ZZ background processes Pythia samples are used. Samples for DY/Z processes are obtained by Alpgen with the Pythia showering model. The modeling of $t\bar{t}$, WZ, ZZ, and DY/Z+HF processes corresponds to the luminosity profile up to the period 17. The samples for the WW and DY/Z processes, with exception of few DY/Z samples, have full luminosity profile. A list of the used MC samples are presented in Tables 4 and 5.

The estimation of the DY/Z background is obtained with a partially data-driven method and performed separately for different decay modes and for different regions of dilepton invariant mass [4]. To perform the estimation, we consider 6 types of non-tagged and 2 types of tagged

CDF Run II Preliminary (8.8 fb^{-1})

$t\bar{t}$ **dilepton sample, tagged events**	
Source	ll
WW	0.57 ± 0.15
WZ	0.12 ± 0.03
ZZ	0.20 ± 0.06
DY+LF	2.4 ± 0.3
DY+HF	2.1 ± 0.2
Fakes	8.6 ± 2.7
Total background	13.9 ± 2.8
$t\bar{t}$ ($\sigma = 7.4$ pb)	227.2 ± 16.2
Total SM expectation	241.1 ± 16.4
Observed	230

Table 2: Summary of expected and observed events in SecVtx b-tagged data sample corresponding to an integrated luminosity of 8.8 fb^{-1}.

CDF Run II Preliminary (9.1 fb^{-1})

$t\bar{t}$ **dilepton sample, 0 tags**	
Source	ll
WW	16.4 ± 3.6
WZ	5.2 ± 1.0
ZZ	3.0 ± 0.5
$Z/\gamma^* \to ee + \mu\mu + \tau\tau$	51.2 ± 8.0
Fakes	21.4 ± 6.2
Total background	97.2 ± 14.5
$t\bar{t}$ ($\sigma = 7.4$ pb)	173.2 ± 13.3
Total SM expectation	270.3 ± 26.4
Observed	290

Table 3: Summary of expected and observed events in non-tagged data sample corresponding to an integrated luminosity of 9.1 fb^{-1}.

DY/Z backgrounds (see Table 5). The model of the fake events is based on weighting of the events from the W+jets data sample according to the fake rate probability matrix [4].

In order to correct for the differences between data and simulation in lepton selection, we calculate the dilepton scale factor SF^{ik}_{2lep} for selected MC events:

$$SF^{ik}_{2lep} = (\epsilon^i_{trig} + \epsilon^k_{trig} - \epsilon^i_{trig} \cdot \epsilon^k_{trig}) \cdot SF^i_{lep} \cdot SF^k_{lep}, \quad (1)$$

where ϵ_{trig} and SF_{lep} are the lepton trigger efficiency and the lepton scale factor. Term $\epsilon^i_{trig} + \epsilon^k_{trig} - \epsilon^i_{trig} \cdot \epsilon^k_{trig}$ in (1) corresponds to the dilepton trigger efficiency for events with lepton types i and k. To correct for the differences between data and simulation in b-tagging we calculate the N-tagging scale factor SF_{Ntag} for MC events with N_{tag} tagged jets:

$$SF_{Ntag} = 1 - (1 - SF_{tag})^{N_{tag}}, \quad (2)$$

where SF_{tag} is the b-tagging scale factor. Also, we have to take into account that the integrated luminosities of the tagged and non-tagged samples, L_{tag} and L_{notag}, are different. In order to introduce the above-described scale factors into our modeling we assume that the selected MC event can simultaneously contribute to the both subsamples. Weights of the MC event in the tagged and non-tagged subsamples, W^{tag}_{MC} and W^{notag}_{MC}, are calculated according to the following formulas:

$$\begin{aligned} W^{tag}_{MC} &= SF_{2lep} \cdot SF_{Ntag} \cdot L_{tag} \\ W^{notag}_{MC} &= SF_{2lep} \cdot (L_{notag} - SF_{Ntag} \cdot L_{tag}). \end{aligned} \quad (3)$$

Instead of the formula (2), the mistag matrix is used to calculate the factor SF_{Ntag} for the DY/Z+LF background. Also, we introduce an additional factor σ_{GEN}/N_{GEN} in the weights of DY/Z events to perform a smooth transition between the samples generated with different parton multiplicities. σ_{GEN} and N_{GEN} are the cross section of sub-process and the number of generated events in sample.

The obtained templates of the considered processes are combined together according to the expected event numbers presented in Tables 2 and 3. In order to validate our modeling we plot different kinematic variables comparing the data to the MC expectation. These plots are shown in Figures 2,...,10.

4 Calculating variable for Top Quark Mass Measurement

4.1 "Hybrid" variable's method

To measure the top quark mass, typically, we can perform the template analysis using a variable sensitive to the top mass. The choice of this variable can be made by the requirement of a minimal expected uncertainty of the measurement. In our analysis we optimize the joint uncertainty that includes two main parts: the statistical and jet the energy scale systematic uncertainties. To achieve this optimization, we use two initial variables with different properties.

Process	**Samples**
$t\bar{t}$, M_{top} =172.5 GeV/c^2	ttop25
$t\bar{t}$, M_{top} =160 GeV/c^2	ttkt60, htktm0
$t\bar{t}$, M_{top} =161 GeV/c^2	ttkt61, htmtmj
$t\bar{t}$, M_{top} =162 GeV/c^2	ttkt62, htktm1
$t\bar{t}$, M_{top} =163 GeV/c^2	ttkt63, htmtmk
$t\bar{t}$, M_{top} =164 GeV/c^2	ttkt64, htktm2
$t\bar{t}$, M_{top} =165 GeV/c^2	ttkt65, ltkt00
$t\bar{t}$, M_{top} =166 GeV/c^2	ttkt66, htktm3
$t\bar{t}$, M_{top} =167 GeV/c^2	ttkt67, htmtmn
$t\bar{t}$, M_{top} =168 GeV/c^2	ttkt68, htktm4
$t\bar{t}$, M_{top} =169 GeV/c^2	ttkt69, htmtmp
$t\bar{t}$, M_{top} =170 GeV/c^2	ttkt70, ltkt02
$t\bar{t}$, M_{top} =171 GeV/c^2	ttkt71, htmtms
$t\bar{t}$, M_{top} =172 GeV/c^2	ttkt72, htktm5
$t\bar{t}$, M_{top} =173 GeV/c^2	ttkt73, htmtmu
$t\bar{t}$, M_{top} =174 GeV/c^2	ttkt74, htktm6
$t\bar{t}$, M_{top} =175 GeV/c^2	ttkt75, otkt49
$t\bar{t}$, M_{top} =176 GeV/c^2	ttkt76, htktm7
$t\bar{t}$, M_{top} =177 GeV/c^2	ttkt77, htmtmz
$t\bar{t}$, M_{top} =178 GeV/c^2	ttkt78, htktm8
$t\bar{t}$, M_{top} =179 GeV/c^2	ttkt79, htktt1
$t\bar{t}$, M_{top} =180 GeV/c^2	ttkt80, ltkt05
$t\bar{t}$, M_{top} =181 GeV/c^2	ttkt81, htmtt4
$t\bar{t}$, M_{top} =182 GeV/c^2	ttkt82, htktm9
$t\bar{t}$, M_{top} =183 GeV/c^2	ttkt83, htmtt6
$t\bar{t}$, M_{top} =184 GeV/c^2	ttkt84, htktma
$t\bar{t}$, M_{top} =185 GeV/c^2	ttkt85, ltkt07

Table 4: The MC samples used for the modeling of $t\bar{t}$ signal

Process	Samples
WW	ftktww
WZ	jhht1a
ZZ	khht1a
$Z/\gamma^* \to ee$ (in Z-window), $Z/\gamma^* \to \mu\mu$ (in Z-window), $Z/\gamma^* \to ee$ (out Z-window), $Z/\gamma^* \to \mu\mu$ (out Z-window), $Z/\gamma^* \to \tau\tau$, $Z/\gamma^* \to \mu\mu$ (as $e\mu$), DY/Z+LF	ztktf0, ztktf1, ztktf2, ztktf3, ztktf4, ztktf5, ztktf6, ztktf7, ztktf8, ztktg0, ztktg1, ztktg2, ztktg3, ztktg4, ztktg5, ztktg6, ztktg7, ztktg8, ztkth0, ztkth1, ztkth2, ztkth3, ztkth4, ztkth5, ztkth6, ztkth7, ztkth8, ztopl0, ztopo0, ztopl1, ztopo1, ztopl2, ztopo2, ztopm0, ztopo3, ztopm1, ztopo4, ztopm2, ztopo5
DY/Z+HF	ztopb0, btopzd, ztopb1, btopze, ztopb2, btopzf, ztopb5, btopzg,ztopb6, btopzh, ztopb7, btopzi, ztopbt, btopzj, xtopb0, xtopb1, xtopb2, xtopb5, xtopb6, xtopb7, xtopbt, ytop0b, ytop1b, ytop2b, ytop5b, ytop6b, ytop7b, ytoptb
Fakes	W+jets data

Table 5: Samples used for the modeling of the background processes.

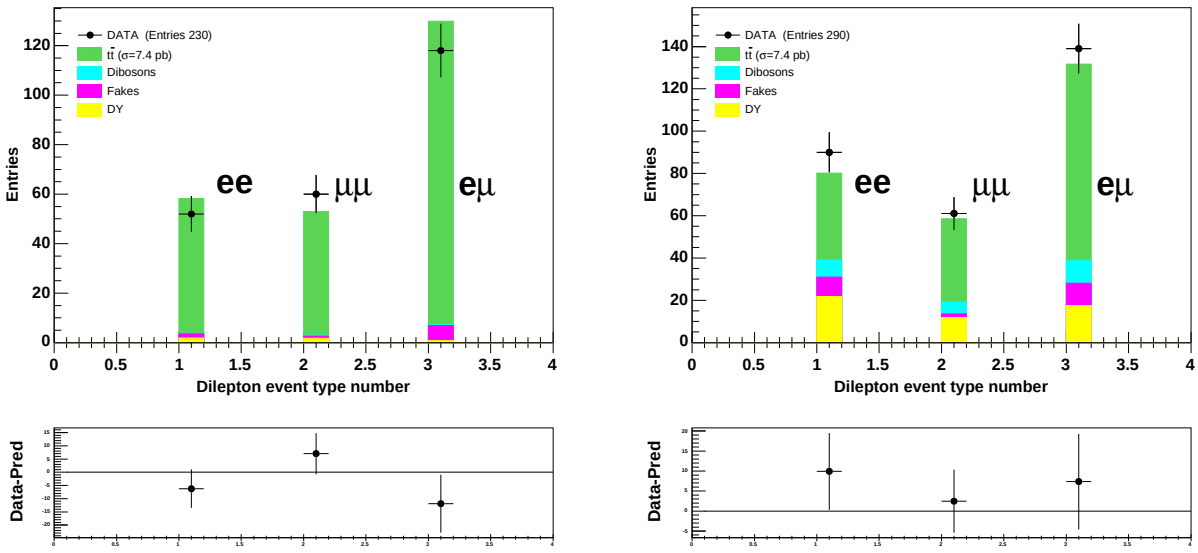

Figure 2: Number of the ee, $\mu\mu$ and $e\mu$ events for the b-tagged (left) and non-tagged (right) subsamples. Data are overlaid with the prediction.

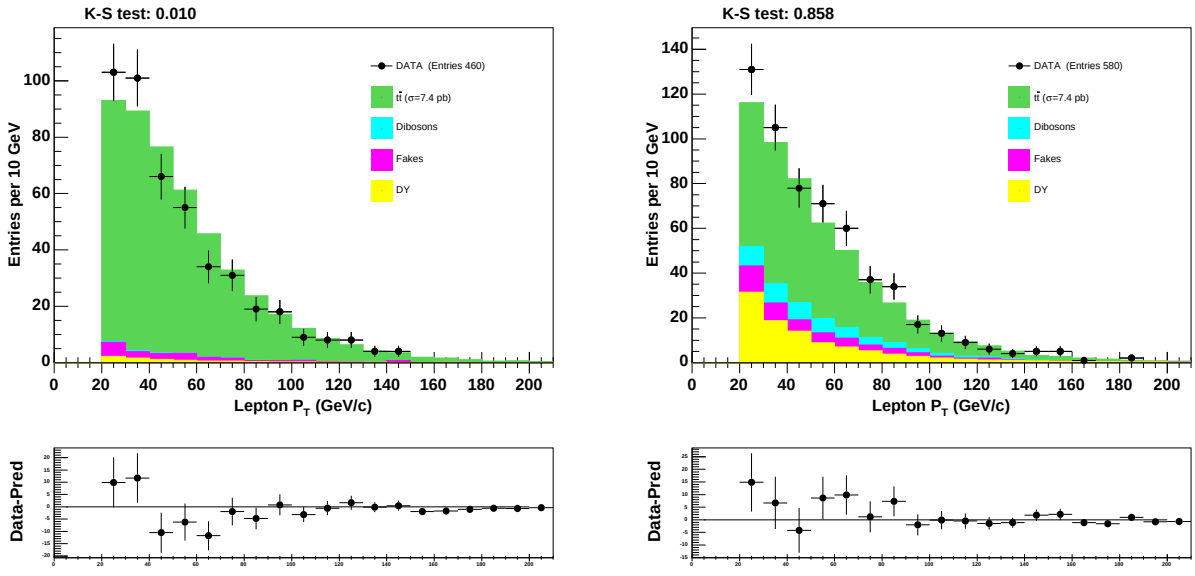

Figure 3: Distribution of the lepton P_T for the b-tagged (left) and non-tagged (right) subsamples. Data are overlaid with the prediction.

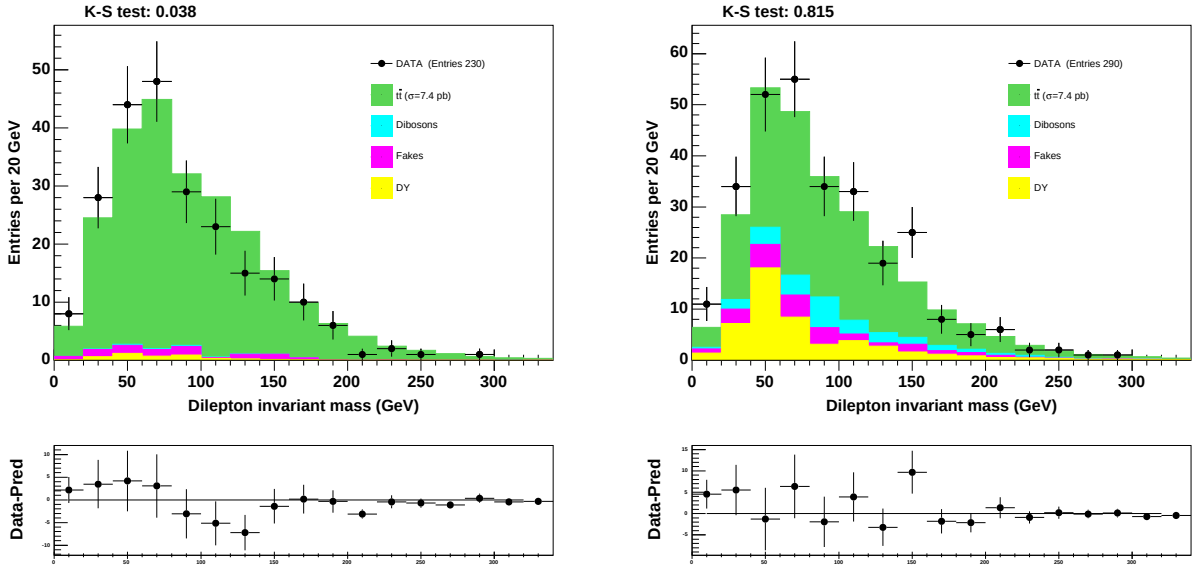

Figure 4: Distribution of the dilepton invariant mass for the b-tagged (left) and non-tagged (right) dilepton subsamples. Data are overlaid with the prediction.

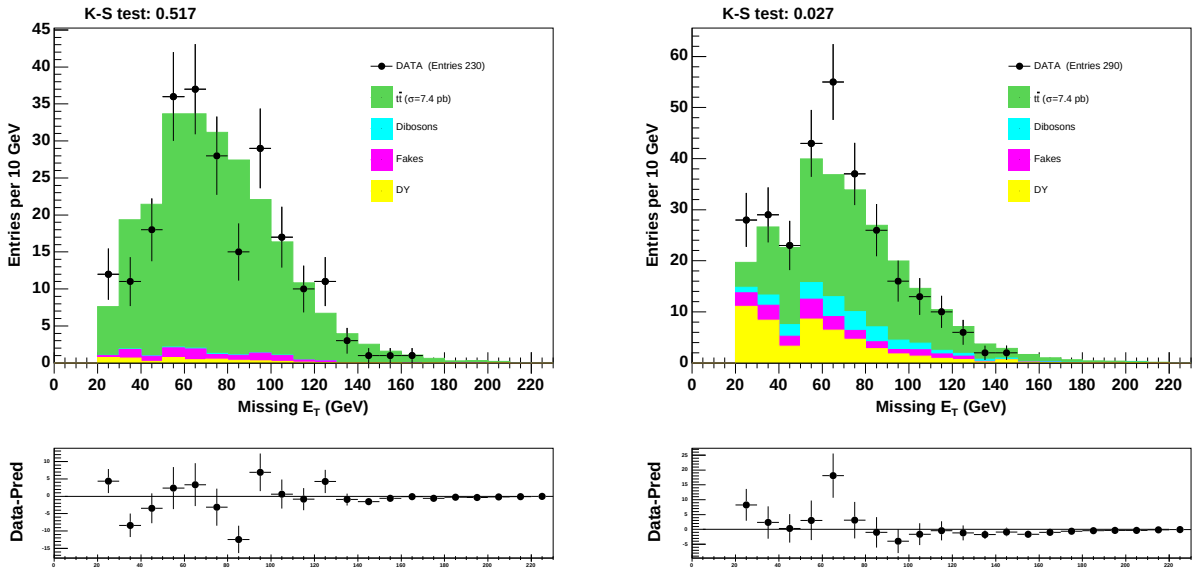

Figure 5: Distribution of the missing E_T for the b-tagged (left) and non-tagged (right) subsamples of the dilepton events. Data are overlaid with the prediction.

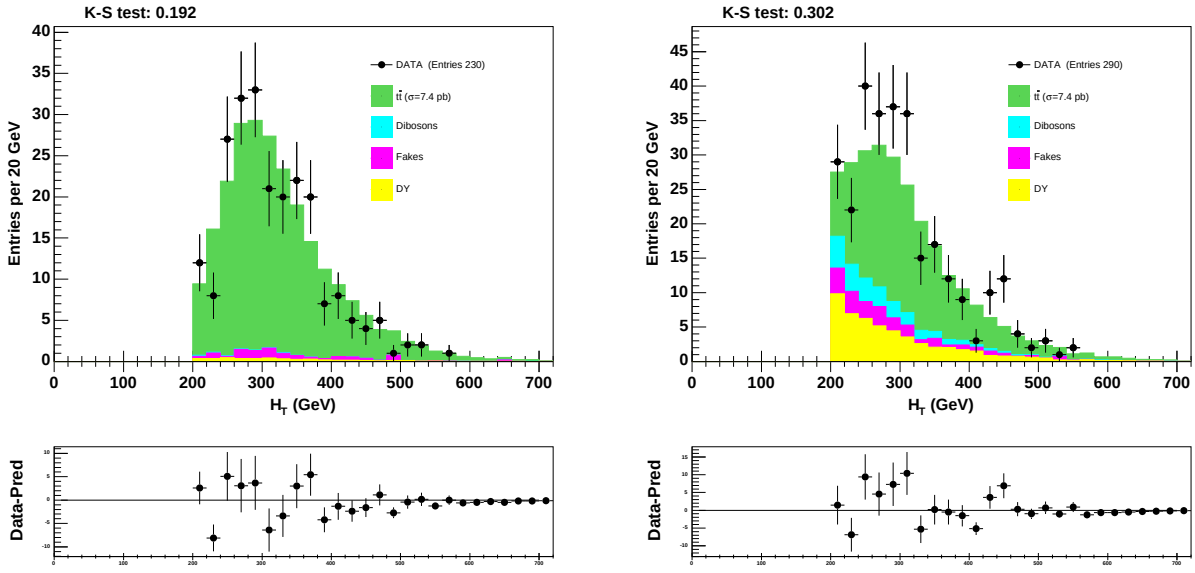

Figure 6: H_T distribution for the b-tagged (left) and non-tagged (right) subsamples of the dilepton events. Data are overlaid with the prediction.

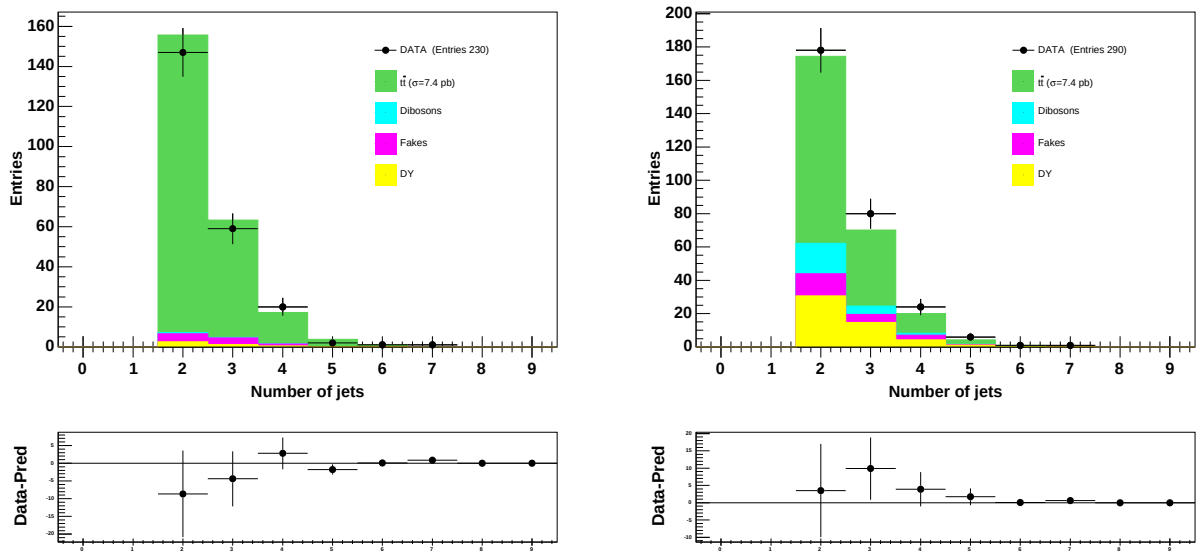

Figure 7: Jet multiplicity distribution for the b-tagged (left) and non-tagged (right) subsamples of the dilepton events. Data are overlaid with the prediction.

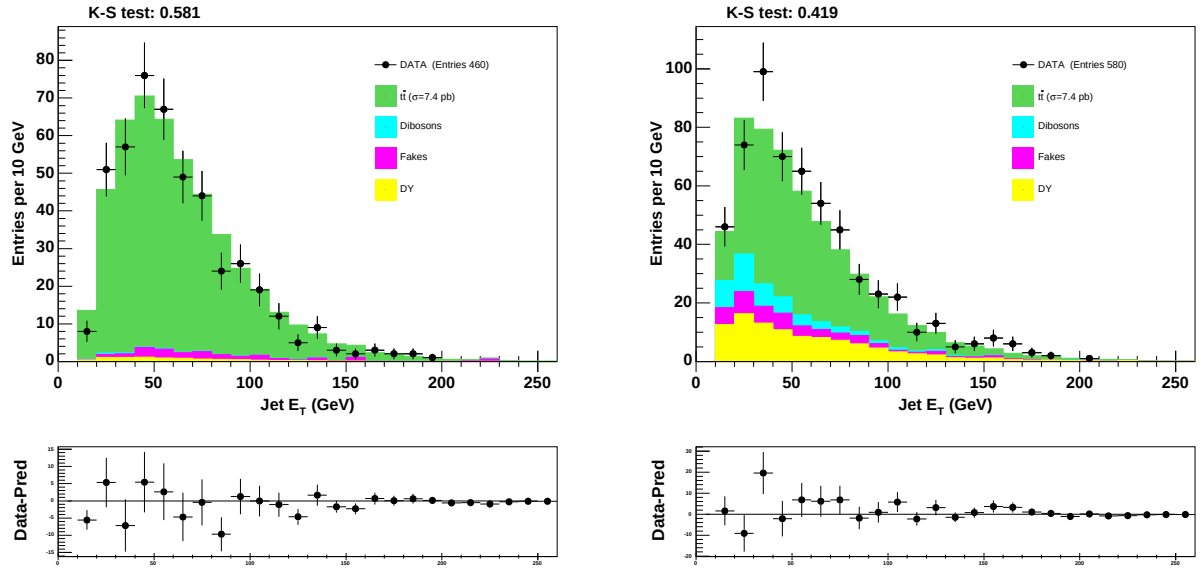

Figure 8: Jet transverse energy distribution for the b-tagged (left) and non-tagged (right) subsamples of the dilepton events. Data are overlaid with the prediction.

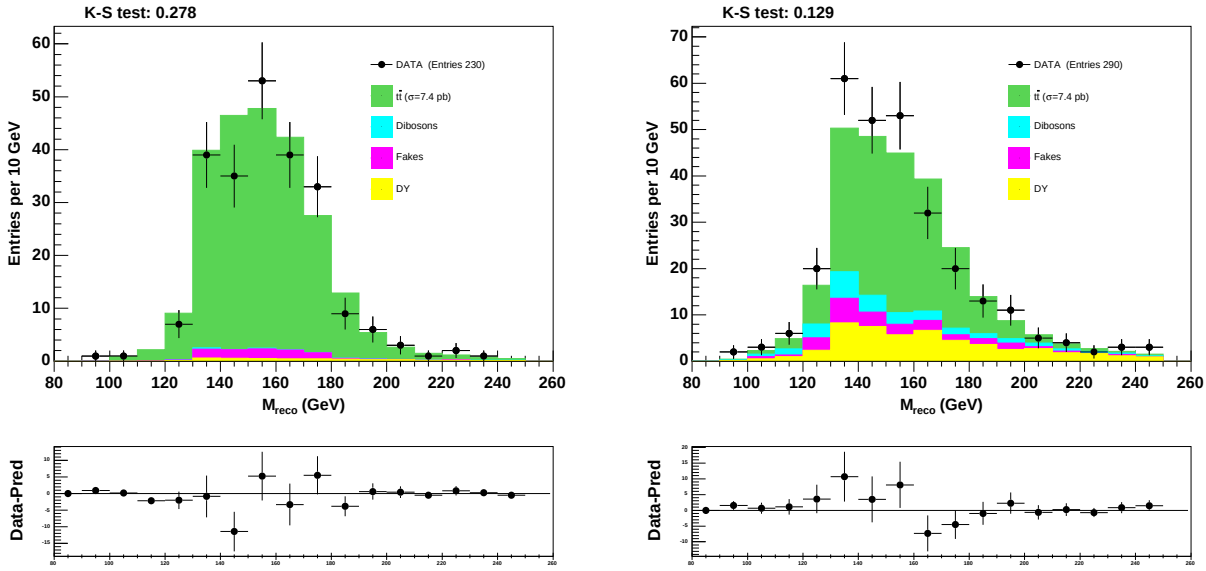

Figure 9: Distribution of reconstructed mass (see Section 4 for definition) for the b-tagged (left) and non-tagged (right) subsamples of the dilepton events. Data are overlaid with the prediction.

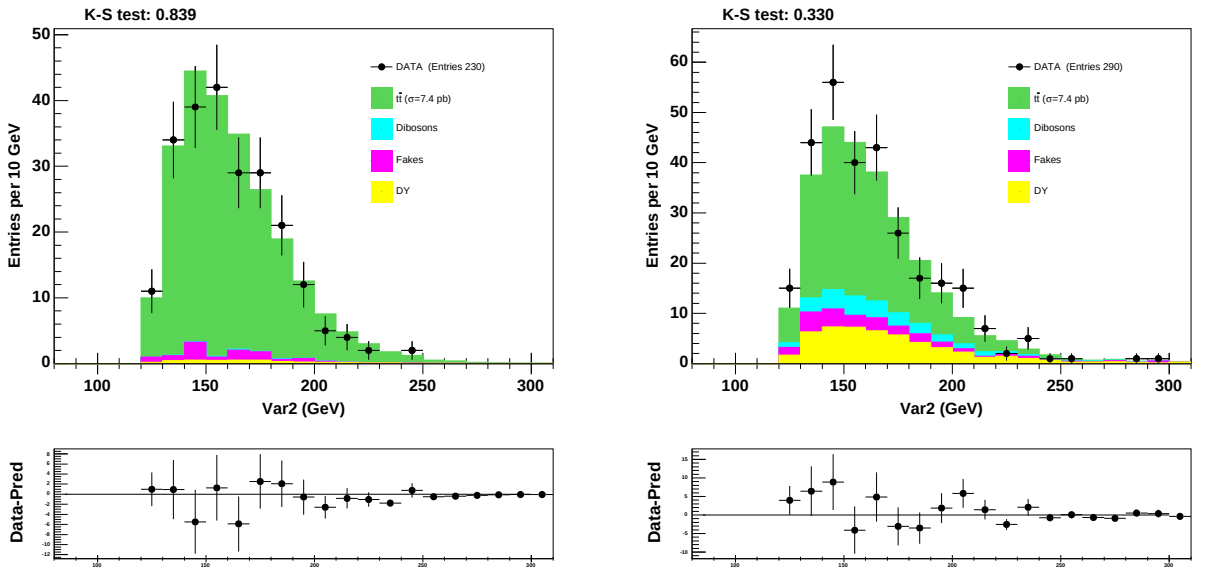

Figure 10: Distribution of M_t^{alt} variable (see Section 4 for definition) for the b-tagged (left) and non-tagged (right) subsamples of the dilepton events. Data are overlaid with the prediction.

First variable is reconstructed mass (M_t^{reco}). It is calculated using the kinematic fit of the dilepton events (see 4.2). and it is the most sensitive variable to the true top mass. In contrast to M_t^{reco}, our second variable is the most sensitive to the top mass, which we can build without using information about jet energies. Therefore, this variable is insensitive to jet energy scale (JES) but it is less sensitive to the top mass if compared to M_t^{reco}. We denote it as "alternative" mass, M_t^{alt}. Details of the M_t^{alt} calculation can be found in Section 4.3. As a next step, we define a "hybrid" variable using a weighted sum of these two variables. In the note we will denote this variable as an effective top mass (M_t^{eff}):

$$M_t^{eff} = w \cdot M_t^{reco} + (1 - w) \cdot M_t^{alt}, \tag{4}$$

where w is the weighting parameter. If we change w from 0 to 1, M_t^{eff}'s properties are smoothly transforming from M_t^{alt}'s to M_t^{reco}'s properties. Therefore, we can choose w in our analysis by the requirement of the minimal expected $stat \oplus JES$ uncertainty of the measurement. The choice of the optimal value of $w = 0.7$ is discussed in Section 4.4.

We choose the "hybrid" variable method as alternative to the best linear unbiased estimator (BLUE) method [6]. In contrast to BLUE, we don't need to combine correlated results because the template method framework automatically accounts for the usage of the right amount of information from the both variables.

4.2 Calculating reconstructed mass

The method implemented in this analysis for reconstructing the top quark mass event by event is called the "Neutrino ϕ Weighting Method". This method was previously used for top quark mass measurement on the lepton+track sample [7].

4.2.1 Neutrino ϕ Weighting Method

In contrast to the lepton plus jets case, in the dilepton channel, we have a non-constrained kinematics due to the existence of two neutrinos. The number of independent variables is more than the number of kinematic constrains: a total number of the unknowns is 24 (b, $\overline{b}$, l^-, l^+, ν and $\overline{\nu}$ 4-momenta) while only 23 kinematic equations can be written (measuring 3-momenta of the two b-jets and two leptons, assuming to know the mass of 6 final particles, used two transverse components of calorimeter missing energy, constrained invariant mass for the two Ws and assumed equal constrained masses of the top and antitop quarks).

In order to constrain the kinematics, the scanning over the space of possibilities for the azimuthal angles of neutrinos ($\phi_{\nu_1}, \phi_{\nu_2}$) is used. A top quark mass is reconstructed by minimizing a chi-squared function (χ^2) in the dilepton $t\overline{t}$ event hypothesis. The χ^2 has two terms:

$$\chi^2 \ = \chi^2_{reso} + \chi^2_{constr} \tag{5}$$

The first term takes into account the detector uncertainties and resolution, whereas the second one constrains the parameters to the known physical quantities given their uncertainties. The first term is expressed as follows:

$$\chi^2_{reso} = \sum_{l=1}^{2} \frac{(P_T^l - \tilde{P_T^l})^2}{{\sigma^l_{P_T}}^2} - 2\sum_{j=1}^{2} \ln(\mathscr{P}_{tf}(\tilde{P_T^j}|P_T^j)) + \sum_{i=x,y} \frac{(UE^i - \tilde{UE^i})^2}{{\sigma_{UE}}^2} \tag{6}$$

where we use tilde ($\sim$) to specify the parameters of the minimization procedure, whereas variables without tilde are representing the measured values. With $\mathscr{P}_{tf}$, we define the transfer function between b-quark and jets: it expresses the probability of measuring a jet transverse momentum P_T^j from a given b-quark with transverse momentum $\tilde{P_T^j}$. The transfer function $\mathscr{P}_{tf}$ are eid, detill, in Section 4.2.2. The sum in the first term is over the two leptons in the event; the second sum loops over the two highest-E_T (leading) jets, which are assumed to originate from the b quarks. After candidate events are selected, the momenta of the leading jets are further corrected for multiple hadron interactions, underlying events, and out-of-cone energy losses.

The third sum runs over the transverse components of the unclustered energy (UE^x, UE^y), which is defined as the sum of the energy vectors from the towers that are not already associated with leptons or the leading jets.

The uncertainties (σ_{P_T}) on the lepton P_T used for electrons (e) and muons (μ) are calculated as [7]:

$$\frac{\sigma^e_{P_T}}{P^e_T} = \sqrt{\frac{0.135^2}{P^e_T[\mathrm{GeV}/c]} + 0.02^2} \tag{7}$$

$$\frac{\sigma^\mu_{P_T}}{P^\mu_T} = 0.0011 \cdot P^\mu_T[\mathrm{GeV}/c] \tag{8}$$

The uncertainty on the transverse components of the unclustered energy (σ_{UE}) is defined as $0.4\sqrt{\sum E_T^{\mathrm{uncl}}}$ [8], where E_T^{uncl} is the scalar sum of the transverse energy excluding two leptons and two leading jets.

The second term in Eq. 5, χ^2_{constr}, constrains the parameters of the minimization procedure through the invariant masses of the lepton-neutrino and the lepton-neutrino-leading jets systems. This term is defined as follows:

$$\begin{aligned}\chi^2_{constr} = &-2\ln(\mathscr{P}_{BW}(m^{l_1,\nu_1}_{inv}|M_W,\Gamma_{M_W})) - 2\ln(\mathscr{P}_{BW}(m^{l_2,\nu_2}_{inv}|M_W,\Gamma_{M_W})) \\ &-2\ln(\mathscr{P}_{BW}(m^{l_1,\nu_1,j_1}_{inv}|\tilde{M}_t,\Gamma_{\tilde{M}_t})) - 2\ln(\mathscr{P}_{BW}(m^{l_2,\nu_2,j_2}_{inv}|\tilde{M}_t,\Gamma_{\tilde{M}_t}))\end{aligned} \tag{9}$$

The parameter $\tilde{M}_t$ is giving the reconstructed top quark mass. The term $\mathscr{P}_{BW}(m_{inv};\ m,\Gamma) \equiv \frac{\Gamma^2 \cdot m^2}{(m^2_{inv} - m^2)^2 + m^2\Gamma^2}$ indicates a relativistic Breit-Wigner distribution function, which expresses the probability that an unstable particle of mass m and width Γ decays into a system of particles with an invariant mass m_{inv}. For M_W and Γ_{M_W}, we use the PDG values. For the top width we use the function

$$\Gamma_{M_t} = \frac{G_F}{8\sqrt{2}\pi} M_t^3 (1 - \frac{M_W^2}{M_t^2})^2 (1 + 2\frac{M_W^2}{M_t^2}) \tag{10}$$

according to Ref. [9].

The longitudinal components of the neutrino momenta are free minimization parameters

while the transverse components are related to $\overrightarrow{\not{E}}$ and to the assumed $(\phi_{\nu_1}, \phi_{\nu_2})$ as follows:

$$\begin{cases} P_x^{\nu_1} \equiv P_T^{\nu_1} \cdot \cos(\phi_{\nu_1}) = \frac{\not{E}_{Tx} \cdot \sin(\phi_{\nu_2}) - \not{E}_{Ty} \cdot \cos(\phi_{\nu_2})}{\sin(\phi_{\nu_2} - \phi_{\nu_1})} \cdot \cos(\phi_{\nu_1}) \\ P_y^{\nu_1} \equiv P_T^{\nu_1} \cdot \sin(\phi_{\nu_1}) = \frac{\not{E}_{Tx} \cdot \sin(\phi_{\nu_2}) - \not{E}_{Ty} \cdot \cos(\phi_{\nu_2})}{\sin(\phi_{\nu_2} - \phi_{\nu_1})} \cdot \sin(\phi_{\nu_1}) \\ P_x^{\nu_2} \equiv P_T^{\nu_2} \cdot \cos(\phi_{\nu_2}) = \frac{\not{E}_{Tx} \cdot \sin(\phi_{\nu_1}) - \not{E}_{Ty} \cdot \cos(\phi_{\nu_1})}{\sin(\phi_{\nu_1} - \phi_{\nu_2})} \cdot \cos(\phi_{\nu_2}) \\ P_y^{\nu_2} \equiv P_T^{\nu_2} \cdot \sin(\phi_{\nu_2}) = \frac{\not{E}_{Tx} \cdot \sin(\phi_{\nu_1}) - \not{E}_{Ty} \cdot \cos(\phi_{\nu_1})}{\sin(\phi_{\nu_1} - \phi_{\nu_2})} \cdot \sin(\phi_{\nu_2}) \end{cases} \quad (11)$$

The minimization procedure described above must be performed for all the allowed values of ϕ_{ν_1}, ϕ_{ν_2} in the $(0, 2\pi) \times (0, 2\pi)$ region. Based on a simulation optimization, we choose a ϕ_{ν_1}, ϕ_{ν_2} grid of 24×24 values as inputs for the minimization procedure. In building the grid we avoid the singular points at $\phi_{\nu_1} = \phi_{\nu_2} + k \cdot \pi$, where k is integer number. Note from Eq. 11 that performing the transformation $\phi_\nu \to \phi_\nu + \pi$ leaves P_x^ν and P_y^ν unchanged, but reverses the sign of P_T^ν. We exclude unphysical solutions ($P_T^{\nu_1} < 0$ and/or $P_T^{\nu_2} < 0$) and choose the solutions which lead to positive transverse momenta for both neutrinos. This decreases the number of grid points to 12×12. For each point, 8 solutions can exist because of the two-fold ambiguity in the longitudinal momentum for each neutrino and the ambiguity on the lepton-jet pairing. Therefore, for each event, we perform 1152 minimizations. Every minimization returns a value of M_{ijk}^{reco} and χ^2_{ijk} $(i, j = 1, \ldots, 12;\ k = 1, \ldots, 8)$. We define $\chi'^2_{ij} = \chi^2_{ij} + 4 \cdot \ln(\Gamma_{M_t})$, which is obtained by using Eq. 9 where $\mathscr{P}_{BW}$ is substituted with $\frac{\Gamma \cdot m^2}{(m^2_{inv} - m^2)^2 + m^2\Gamma^2}$, and select the lowest χ'^2 solution for each point of the $(\phi_{\nu_1}, \phi_{\nu_2})$ grid, thereby reducing the number of obtained masses to 144. Each mass is weighted according to

$$w_{ij} = \frac{e^{-\chi'^2_{ij}/2}}{\sum_{i=1}^{12} \sum_{j=1}^{12} e^{-\chi'^2_{ij}/2}} \quad (12)$$

In the next step, we build a mass distribution to define the most probable value (MPV). Masses below a threshold of 30% of the MPV bin content are discarded, and the remaining ones are averaged to compute the preferred top quark mass for the event M_t^{reco}.

4.2.2 Transfer Functions

Since the jet energy corrections have been calibrated on samples dominated by light quarks and gluons, we need an additional correction for a better reconstruction of b-quark jets. In Equation 6, we introduced the transfer functions $\mathscr{P}_{tf}$, which allow us to step back from jets to partons. These functions of jet P_T and η are defined as the parametrization of $\xi \equiv (P_T^{b-quark} - P_T^{jet})/P_T^{jet}$ distributions, built from a large sample of simulated $t\bar{t}$ events. We exploit only jets within a cone of $R = 0.4$ around the generated b quarks. The influence of b-quark P_T-spectra on ξ distributions is excluded by choosing the weights inversely proportional to the probability density of $P_T^{b-quark}$.

In order to parameterize the above distributions we use the following formula:

$$\mathscr{W}_{TF}(\xi) = \frac{\gamma_7\gamma_6}{\sqrt{2\pi}\gamma_2}\, e^{-0.5(\frac{\xi-\gamma_1}{\gamma_2}+\exp(-\frac{\xi-\gamma_1}{\gamma_2}))} + \frac{\gamma_7(1-\gamma_6)}{\sqrt{2\pi}\gamma_5}\, e^{-0.5(\frac{\xi-\gamma_4}{\gamma_5})^2} + \\ + \frac{(1-\gamma_7)}{\sqrt{2\pi}\gamma_3}\, e^{-0.5(\frac{\xi-\gamma_8}{\gamma_3})^2} \quad (13)$$

The parameters $\gamma_1 \cdots \gamma_8$ are obtained by the fit. The distributions are constructed in three bins of $|\eta|$: $|\eta| < 0.7$, $0.7 < |\eta| < 1.3$, and $1.3 < |\eta| < 2.5$, and bins of jet P_T 10 GeV/c wide starting at 30 GeV/c up to 190 GeV/c for $|\eta| < 0.7$, up to 150 GeV/c for $0.7 < |\eta| < 1.3$, and up to 110 GeV/c for $1.3 < |\eta| < 2.5$, and a single bin for above and below these regions. Figure 11 shows the distributions along with the transfer functions for a number of $(|\eta|, P_T^{jet})$ regions.

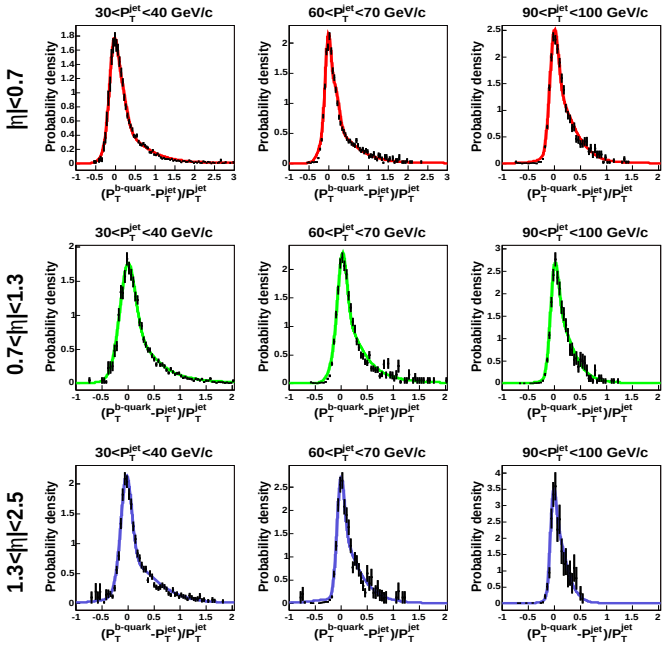

Figure 11: Transfer functions of b-quarks into jets. These functions of jet P_T and η are defined as the parametrization of $(P_T^{b-quark} - P_T^{jet})/P_T^{jet}$ distributions. The points are from the simulated $t\bar{t}$ events. The curves show the best fit with Eq. 13.

4.3 Calculating variable insensitive to JES

In order to define M_t^{alt} as the variable insensitive to JES, we should not use the values of the jet energies. In this case we can exploit only the following experimental information: the 4-momenta (l_1 and l_2) of the leptons and the jet's directions. We can specify the track direction of particle p with the following vector $\vec{c}_p$:

$$\vec{c}_p \equiv (c_x^p, c_y^p, c_z^p), \quad (14)$$

where c_x^p, c_y^p, and c_z^p are the direction cosines of the particle momentum. Also, to operate within a 4-vector scheme, we define the following 4-vector c_p:

$$c_p \equiv (1, \vec{c_p}). \tag{15}$$

We can interpret c_p as 4-momenta of a massless particle with energy of 1 GeV that has the same flight direction as p in the laboratory coordinate system. And, using c_p, we can write our definition for M_t^{alt} by formula:

$$M_t^{alt} \equiv \sqrt{\langle l_1, c_{b_1}\rangle \cdot \langle l_2, c_{b_2}\rangle} + 120 \text{ GeV}, \tag{16}$$

where c_{b_1} and c_{b_2} are 4-vectors deriving from two leading jets. In formula (16), a notation like $\langle l,c\rangle$ means the scalar product of two 4-vectors l and c. From the two possibilities assignments of the leptons and jets in (16), we choose one with maximal value of $\langle \vec{c_{l_1}}, \vec{c_{b_1}}\rangle + \langle \vec{c_{l_2}}, \vec{c_{b_2}}\rangle$ (notation $\langle \vec{c_1},\vec{c_2}\rangle$ means the scalar product of two 3-dimensional vectors $\vec{c_1}$ and $\vec{c_2}$). This criterion gives the correct assignment in about 60% of simulated $t\bar{t}$ events. For the variable M_t^{alt} (16), we apply an additional shift of 120 GeV, which has no impact on our analysis. It is introduced for convenience to equalize the x-axes of the M_t^{alt} and M^{reco} variables in (4).

Eq. 16 is equivalent the next formula:

$$M_t^{alt} \equiv \sqrt{\frac{\langle l_1, b_1\rangle \cdot \langle l_2, b_2\rangle}{E_{b_1} E_{b_2}}} + 120 \text{ GeV}, \tag{17}$$

where b_1 and b_2 are 4-momenta of two leading jets, which are defined in the assumption of massless particles with energies E_{b_1} and E_{b_2}.

4.4 Optimizing the measurement

In order to find the optimal value of w (Eq. 4), we scan the interval of [0,1] with a step of 0.05. In every point of the scan, we build the signal and background templates for M_t^{eff}, define the likelihood function and perform pseudo-experiments (PE's). The PE's procedure is described in the next Sections of this note. We perform a check that the top mass and its error returned from PE's are correct by examining the PE's pulls . We define the expected statistical error as the mean of the error distribution obtained from PE's with $M_{top} = 172.5$ GeV. We define the JES systematic error by applying JES shifts according to the nominal procedure approved for the JES systematic uncertainty (see Section 6.1). The obtained results are shown in Figure 12.

It can be seen that the JES systematic error does not equal to zero at $w = 0$ as we would expect. This is an effect from increasing or decreasing the events in the sample after shift in JES due to the fact that JES is involved in the event selection. Instead of this, the JES systematic uncertainty equals to zero at $w \cong 0.12$. At this point, we have a full compensation of two effects related to JES: changing of the template shape is compensated by the effect of the acceptance changing. These two mechanisms have the different signs and impact differently the top-mass measurement. Typically, the first effect is bigger and is compensated partially by the second one. In the region when we choose smaller values of the w parameter, the second effect can compensate or even overpower the first one.

From Fig. 12, we can conclude that the minimal value of the statistical and the *stat⊕JES* uncertainty corresponds to a value of w=0.5. In the analysis, we have decided to use a value of

$w = 0.7$. At $w = 0.7$, the *stat*$\oplus$*JES* uncertainty has an unessential difference from the minimum of about 2% while the expected statistical uncertainty is notably better. As a general rule, we prefer to avoid increasing of the statistical uncertainty because it can increase also systematic uncertainties from the sources described at Sec. 6. By selecting w=0.7, the expected *stat*$\oplus$*JES* uncertainty is reduced by 12% in a comparison with the case if we would use only the M_t^{reco} variable.

In addition, we would like to discuss the effect on the JES systematics by including the background in event sample. In order to check this effect we compare values of the JES uncertainty that are obtained with "signal+background" and "signal only" PE's cases. For w=0.7 these values equal to 2.42±0.04 GeV and 2.55±0.04 GeV respectively. The obtained result can be interpreted that we do not observe a strong influence from the background on the JES systematic uncertainty (5.0%±2.4%) because the tagged sample has the biggest weight of about 70% in the total result. The comparison of the JES systematic uncertainty for the cases of the tagged and non-tagged samples (2.61±0.04 GeV and 2.15±0.04 GeV respectively) shows a noticeable difference, which can be explained by the different S:B ratio in these samples.

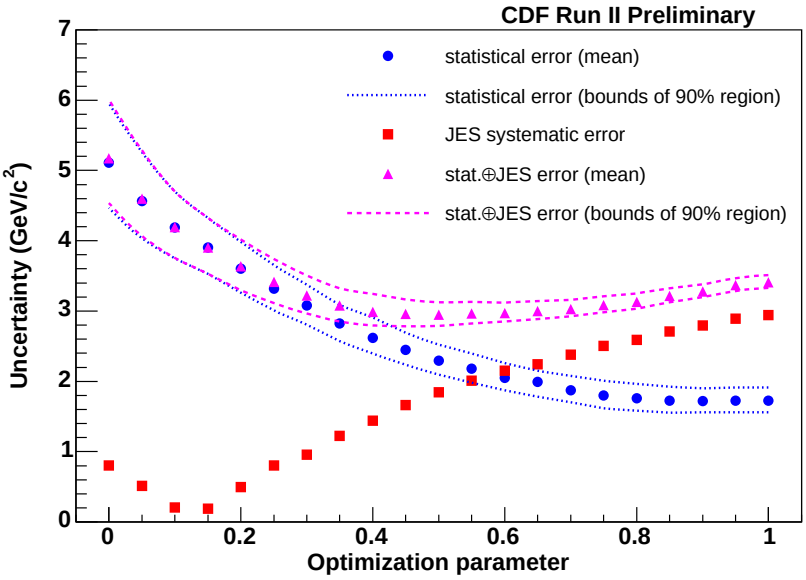

Figure 12: The statistical, JES systematic and *stat*$\oplus$*JES* uncertainties of top-quark mass measurement as function of teh parameter w in Eq. 4.

5 Top Quark Mass Determination

5.1 Templates

The selected data sample is a mixture of signal and background events. In order to extract the top-quark mass, the effective top-mass distribution (see Eq. 4) in the data is compared with

probability density functions (p.d.f.'s) for the signal and background processes and the mass is extracted by a likelihood fit. P.d.f.'s are defined from the parametrizations of templates.

The signal templates are built from $t\bar{t}$ samples generated with PYTHIA for top-quark masses in the range 160 to 185 GeV/c^2 in 1 GeV/c^2 steps. They are parameterized separately for b-tagged and non-tagged events by using a combination of two Landau and one Gaussian distribution functions, as:

$$P_s(M_t^{eff}|M_t) = \frac{p_8 p_7}{\sqrt{2\pi}p_1} e^{-0.5(\frac{M_t^{eff}-p_2}{p_1}+\exp(-\frac{M_t^{eff}-p_2}{p_1}))} + \frac{p_8(1-p_7)}{\sqrt{2\pi}p_3} e^{-0.5(\frac{M_t^{eff}-p_4}{p_3})^2} + \frac{(1-p_8)}{\sqrt{2\pi}p_5} e^{-0.5(\frac{M_t^{eff}-p_6}{p_5}+\exp(-\frac{M_t^{eff}-p_6}{p_5}))} \quad (18)$$

the p.d.f.'s for the signal, P_s^{tag} and P_s^{notag}, express the probability that a effective top mass M_t^{eff} originates from an event with true top-quark mass, M_t. The parameters $p_1, \ldots, p_8$ have an additional dependence from the true top quark mass M_t. These parameters are calculated as:

$$p_k = \alpha_k + \alpha_{k+8} \cdot (M_t[\text{GeV}/c^2] - 175) \quad k = 1, \ldots, 8 \quad (19)$$

The parameters α_k are defined by the signal templates fit. Figures 13 and 14 show a subset of templates along with their parametrizations (solid lines) for the b-tagged and non-tagged templates.

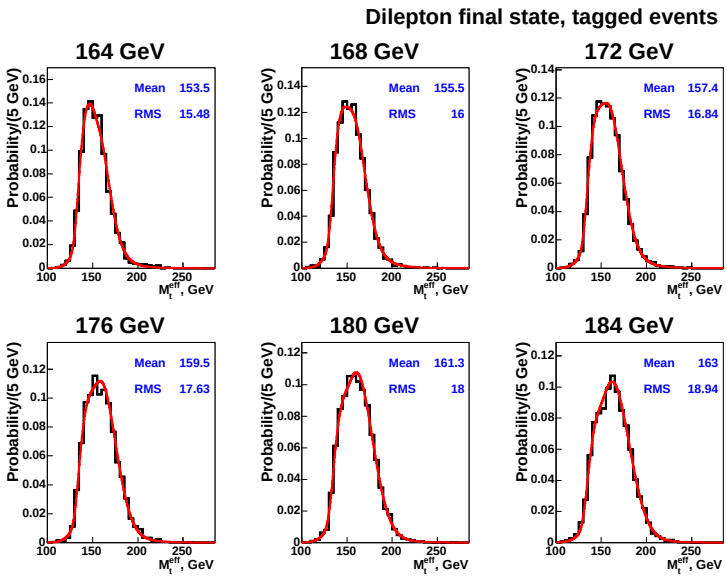

Figure 13: The signal templates and fit result (solid lines) for the b-tagged events and for different input top-quark masses. The parametrization is defined in Eq. 18.

The representative background templates are built separately for b-tagged and non-tagged events by a weighted sum of the templates from diboson, fakes, and Drell-Yan precesses. These templates have been normalized to the expected rates reported in Tables 2 and 3. The fakes template is built from W+jets data events by weighting each event according to the probability

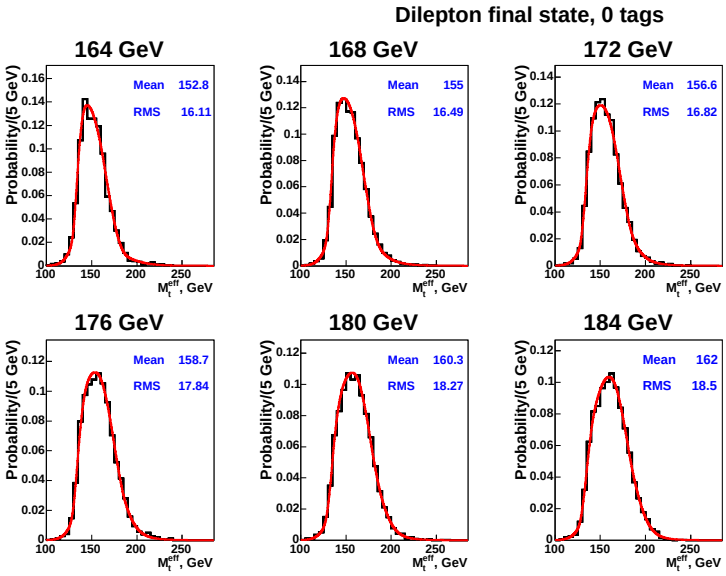

Figure 14: The signal templates and fit result (solid lines) in the non-tagged events for different input top-quark masses. The parametrization is defined in Eq. 18.

for a jet to be mis-identified as a lepton (fake rate). Drell-Yan and diboson templates are built from simulated samples (see Section 3 for details). The combined background templates are fitted with a sum of two Landau and one Gaussian distribution functions, as:

$$P_b(M_t^{eff}) = \frac{\beta_8\beta_7}{\sqrt{2\pi}\beta_1}\, e^{-0.5(\frac{M_t^{eff}-\beta_2}{\beta_1}+\exp(-\frac{M_t^{eff}-\beta_2}{\beta_1}))} + \frac{\beta_8(1-\beta_7)}{\sqrt{2\pi}\beta_3}\, e^{-0.5(\frac{M_t^{eff}-\beta_4}{\beta_4})^2} + \frac{(1-\beta_8)}{\sqrt{2\pi}\beta_5}\, e^{-0.5(\frac{M_t^{eff}-\beta_6}{\beta_5}+\exp(-\frac{M_t^{eff}-\beta_6}{\beta_5}))} \quad (20)$$

where the fitted parameters $\beta_1 \cdots \beta_8$ are M_t-independent. The combined background templates and their parametrization (solid line), Drell-Yan, diboson, and fakes templates are plotted in Figures 15 and 16.

5.2 Likelihood Form

The top mass is extracted from the data sample by performing an unbinned likelihood fit. We define the likelihood function as product of independent likelihoods defined for b-tagged and non-tagged subsamples:

$$\mathscr{L}^{total} = \mathscr{L}^{tag} \cdot \mathscr{L}^{notag}. \quad (21)$$

The likelihood functions, $\mathscr{L}^{tag}$ and $\mathscr{L}^{notag}$, express the probability that a effective top-mass distribution from data is described by a mixture of background and $t\bar{t}$ events with an assumed top-quark mass. The inputs for the likelihood are the values of the effective top masses from data events, the signal and background p.d.f.'s and the expected number of background

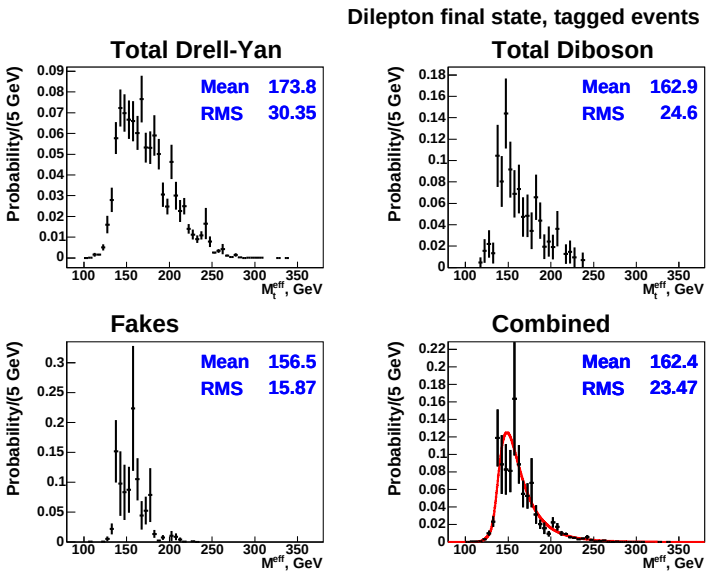

Figure 15: Drell-Yan, fakes, diboson and combined background templates for b-tagged events. The fitting function (solid line), defined in Eq. 20, is superimposed to the combined template.

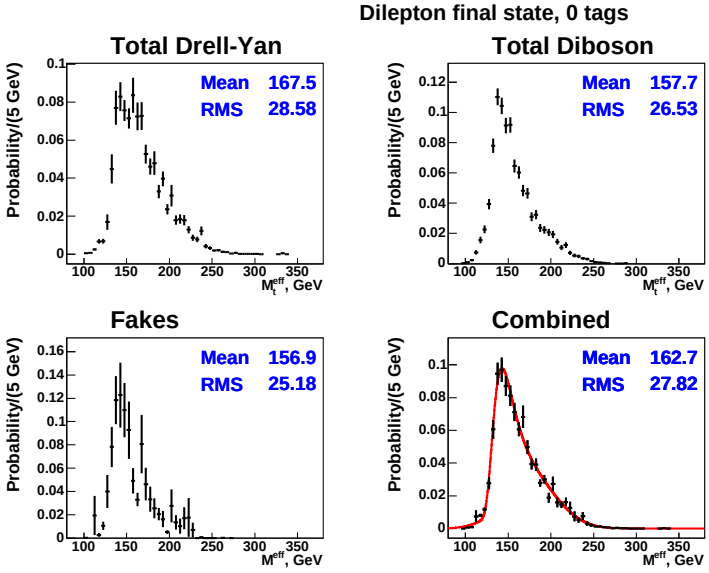

Figure 16: Drell-Yan, fakes, diboson and combined background templates for non-tagged events. The fitting function (solid line), defined in Eq. 20, is superimposed to the combined template.

events. The latter ($n_b^{exp\ tag}$=13.92 and $n_b^{exp\ notag}$=97.16) and their errors ($\sigma_{n_b^{exp\ tag}}$=2.85 and $\sigma_{n_b^{exp\ notag}}$=15.14) are taken from Tables 2 and 3. The likelihoods,$\mathscr{L}^{tag}$ and $\mathscr{L}^{notag}$, have the same form:

$$\mathscr{L} = \mathscr{L}_{shape} \cdot \mathscr{L}_{backgr}; \tag{22}$$

where

$$\mathscr{L}_{shape} = \frac{e^{-(n_s+n_b)} \cdot (n_s+n_b)^N}{N!} \cdot \prod_{n=1}^{N} \frac{n_s \cdot P_s(M_t^{eff}|M_{top}) + n_b \cdot P_b(M_t^{eff})}{n_s+n_b}, \tag{23}$$

$$\mathscr{L}_{backgr} = \exp(\frac{-(n_b - n_b^{exp})^2}{2\sigma^2_{n_b^{exp}}}). \tag{24}$$

The shape likelihood term, $\mathscr{L}_{shape}$ (Eq. 23), expresses the probability of an event being a signal with the top mass of M_{top} or a background. The signal (P_s) and the background (P_b) probabilities are weighted according to the number of signal (n_s) and background (n_b) events, which are floated in the likelihood fit. In the fitting procedure, n_b is constrained to be Gaussian-distributed with mean value n_b^{exp} and standard deviation $\sigma_{n_b^{exp}}$, as shown by Eq. 24, while $(n_s + n_b)$ is the mean of N Poisson distributed events.

We perform the likelihood fit using the MINUIT [10] program. Fit returns the estimated top-quark mass (M_{top}^{fit}) and the estimated numbers of the signal ($n_s^{tag\ fit}$ and $n_s^{notag\ fit}$) and the background ($n_b^{tag\ fit}$ and $n_b^{notag\ fit}$) events. M_{top}^{fit} returned by the likelihood fit is the mass corresponding to the minimum of the $[-\ln \mathscr{L}^{total}]$ function. The positive and negative statistical uncertainties are the difference between M_{top}^{fit} and masses at $[-ln(\mathscr{L})]_{min} + 0.5$. The positive and negative statistical errors (σ^+ and σ^-) are returned by MINOS [10]. The final result is presented with the symmetrized statistical error: $\sigma = (\sigma^+ + |\sigma^-|)/2$.

5.3 Bias checks

We checked whether our likelihood fit (21) is able to return the correct mass. The checks are performed by running a large number (2500) of PE's on simulated background and signal events where the true top quark mass is known. Each PE consists of signal (N_s^{PE}) and background (N_b^{PE}) events, drawn from a signal and background template, and performing the likelihood fit, as described in Sec. 5.2. A top quark mass (M_t^{fit}) and its statistical errors are returned too. Numbers of signal and background events are generated according to Poisson distributions with means given in Tables 2 and 3.

For each input mass, the median of the M_t^{fit} distribution is chosen as the top-quark mass estimate (M_t^{out}). M_t^{out} versus input mass (M_t) and the bias, defined as $M_t^{out} - M_t$, are shown in Figure 17. The error bars are determined by the limited statistics of the signal templates. The fits in Figure 17 are performed in the mass range 160-185 GeV/c^2. The slope of the straight line in the upper plot is consistent with one, while the average bias (horizontal line in the lower plot) is consistent with zero. This result confirms that the obtained top quark mass M_{top}^{fit} is unbiased and we do not need to apply any additional corrections to the output from the LH fit.

In order to check the bias on the statistical error we use pulls. Pulls are defined as follows:

$$\frac{M_t^{fit} - M_t}{\sigma}. \tag{25}$$

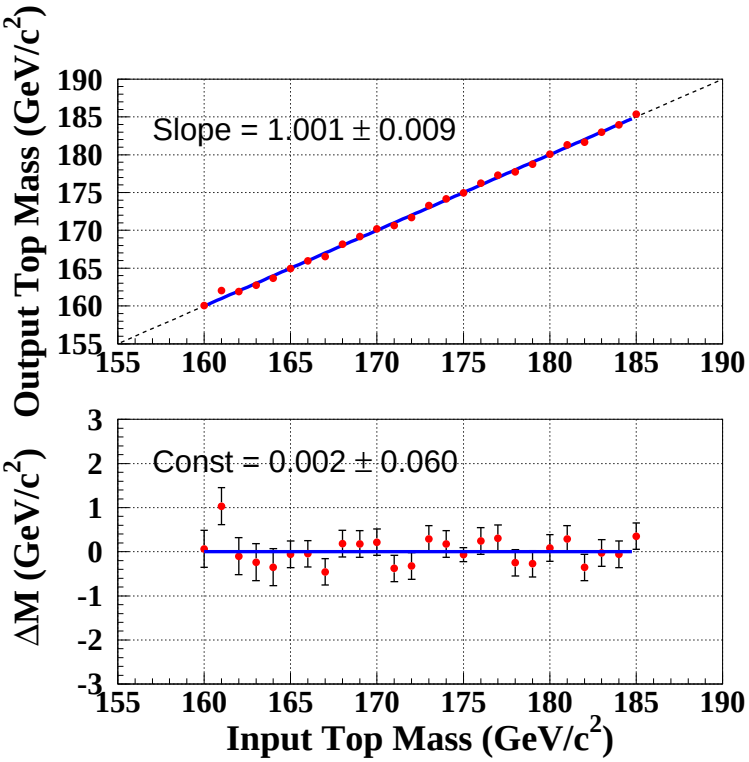

Figure 17: Results from PE's. The upper plot shows M_t^{out} versus input masses, while the lower one shows the bias.

For each generated top quark mass, pull distributions are fitted by using Gaussian functions (some examples are shown in Figure 18). The width of the pull distributions versus the generated top quark mass are shown in Figure 19. Error bars account for the limited statistics of the templates. The average width of the pull distributions can be considered compatible with one within the uncertainties. Accordingly, there is no need to re-scale the statistical uncertainty obtained from data.

We estimated the expected statistical uncertainty of the top-quark mass measurement using sample of simulated $t\bar{t}$ events with the input mass of 172.5 GeV/c^2 (see Figure 20). The expected error is 1.87 GeV/c^2.

6 Systematic Uncertainties

Since the method compares data to expectations estimated from Monte Carlo simulations, uncertainties in our model used to generate events may cause systematic uncertainties. Other systematic uncertainties arise from the potential mis-modeling of the background template shape.

We calculate the contribution to the systematics from each source of uncertainty according to the Top Mass Group prescriptions [11]. The generic procedure for estimating a systematic uncertainty can be described as follows: the parameters used for the generation of events are

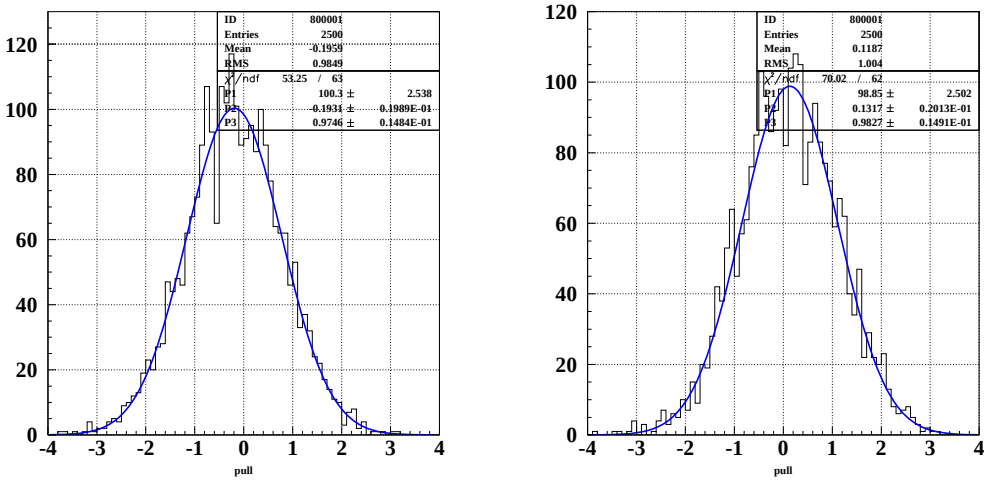

Figure 18: Results from PE's: pull distributions for generated mass samples at M_t = 171 GeV/c^2 (left) and M_t = 172.5 GeV/c^2 (right). The distributions are fit to a Gaussian p.d.f (solid line).

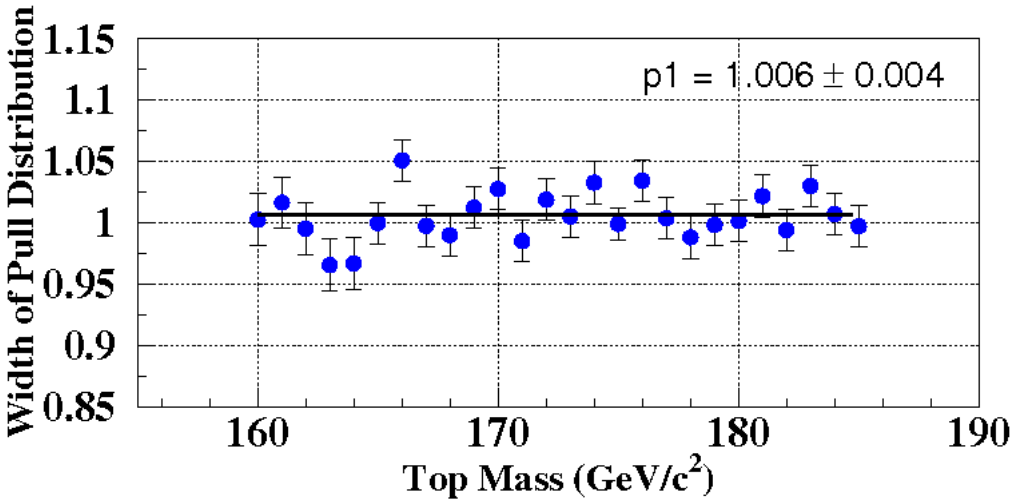

Figure 19: Results from PE's: width of the pull distributions versus generated top-quark mass.

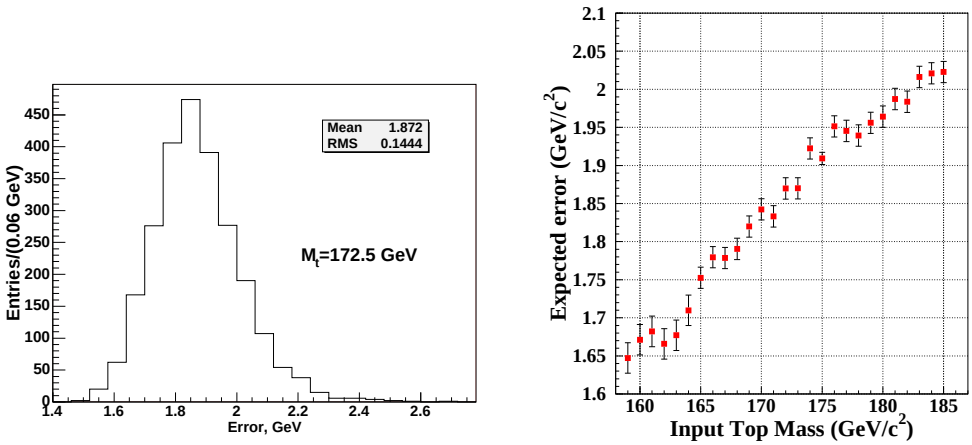

Figure 20: Results from PE's: (left) statistical error distribution for the top-quark mass measurement using the MC sample with mass of 172.5 GeV/c^2 and (right) expected statistical uncertainty of the measurement versus the input top mass.

modified (by $\pm$ 1 standard deviation) and new templates are built. PE's from the modified templates are performed and using for the event reconstruction the same p.d.f.'s as in the nominal analysis. The difference between the median of the top-quark mass distribution obtained from the shifted PE's and the nominal top quark mass is used for an estimation of the systematic uncertainty.

All sources of systematic uncertainties are assumed to be uncorrelated to each other, so the overall systematic uncertainty is obtained by adding in quadrature the individual uncertainties. The systematic uncertainties along with the total uncertainty are summarized in Table 17. The total systematic uncertainty is estimated to be 2.69 GeV/c^2. In the following, we describe how each of the systematic uncertainties is evaluated.

6.1 Jet energy scale

The energy assigned to jets is corrected according to the calorimeter response. Jet corrections correct for the non-uniformity in calorimeter response as a function of $|\eta|$, effects of multiple $p\bar{p}$ collisions, the hadronic jet energy scale, deposited energy due to underlying events, and out-of-cone energy lost in the clustering procedure. The systematic uncertainty due to the jet energy scale (JES) is estimated from signal and background events in which each jet energy correction has been shifted by $\pm$ 1 standard deviation inside its uncertainty interval. Shifted signal and background templates are built and then two sets of PE's are performed. The top-quark masses (M_t^+ and M_t^-) are estimated as the medians of the mass distributions. The systematic uncertainty for each level of corrections is taken as $(M_t^+ - M_t^-)/2$. The individual uncertainties are summed in quadrature in order to obtain the JES systematic uncertainty. The results are reported in Table 6.

Level	Source	M_t (GeV/c^2)		Uncertainty (GeV/c^2)
		$+\sigma^{JES}$	$-\sigma^{JES}$	$(M_t^+ - M_t^-)/2$
1	η-dependent	173.216	172.301	0.458 ± 0.026
4	Multiple interactions	172.944	172.762	0.091 ± 0.026
5	Absolute scale	174.566	171.152	1.707 ± 0.026
6	Underlying event	172.968	172.615	0.177 ± 0.026
7	Out-of-cone	174.479	171.226	1.627 ± 0.026
8	Splash-out	173.063	172.551	0.256 ± 0.026
	Sum in quadrature			2.42 ±0.06
Total JES systematics				**2.4**

Table 6: Systematic uncertainties on the top-quark mass for each level of the jet energy correction. The total uncertainty is the sum, in quadrature, of the individual uncertainties.

6.2 b-jet energy scale

Since jet energy corrections are estimated with studies dominated by light-quarks and gluon jets, additional uncertainty occurs on the b-jet energy scale. There are three main reasons:

1. uncertainty in the heavy-flavor fragmentation model;
2. uncertainty in the b-jet semileptonic branching ratio;
3. uncertainty in the calorimeter response of b-jets.

The effect on the measured top quark mass of the fragmentation model is evaluated by re-weighting events according to two different fragmentation models from fits on LEP(ADO) and SLD data [11]. Shifted templates are built and PE's are performed to define the mass shifts. The results from PE's are shown in Table 7. In both cases the mass shifts from nominal are consistent with zero within uncertainties. So, we take the uncertainty of the mass shift (0.05 GeV/c^2) as our estimation of this systematics, according to the top-mass group prescription.

The effect for the uncertainty in the semileptonic branching ratios (BRs) of heavy flavor quarks is evaluated by shifting BRs by $\pm\sigma$. Events are re-weighted accordingly and shifted templates are built. Results from PE's are shown in Table 7. We get a value of 0.26 GeV/c^2 as systematics due to this source of uncertainty.

The effect of the uncertainty due to the b-jet energy calorimeter response is estimated by shifting the jet energy scale for every jets identified to steam from b-quarks. We shift the b-JES by $\pm 1\%$. Shifted templates are built and PE's are performed to define the mass shifts (see Table 7). According to the prescription [11] we take 20% of the half difference as systematic uncertainty.

All above uncertainties are added in quadrature to get the value of the total b-JES systematic uncertainty of 0.34 GeV/c^2.

Source of uncertainty	Datasets	Comment	Mass, GeV/c^2	Mass Shift, GeV/c^2	Syst. GeV/c^2
Fragmentation model	ttkt75+otkt49	nominal	174.935±0.036		0.05
		ADO	174.949±0.036	ΔM=0.014±0.051	
		SLD	174.901±0.036	ΔM=-0.034±0.051	
b-jet semileptonic branching ratio	ttop25	nominal	172.721±0.036		0.28
		$+\sigma^{BR}$	172.429±0.036	$\Delta M/2$=	
		$-\sigma^{BR}$	172.989±0.036	0.280±0.026	
b-jets energy response in colorimeter	ttop25	+1% in b-JES	173.684±0.036	$\Delta M/2$ =	0.2*0.903
		-1% in b-JES	171.877±0.036	0.903±0.026	=0.18
Total b-JES systematic error					**0.34**

Table 7: Systematics for the b-JES.

6.3 Lepton energy scale

The effect on the top mass from the uncertainty on the lepton energy scale is studied by applying ±1% shifts for the electron and muon energy scale. Shifted templates are built and PE's are performed to define the mass shifts. The results from PE's are shown in Table 8. The shifts in top mass due to uncertainties in the electron and muon energy scales are added in quadrature to obtain the value of the lepton energy uncertainty of 0.36 GeV/c^2.

Source of uncertainty	Datasets	Comment	Mass, GeV/c^2	Mass Shift, GeV/c^2	Syst. GeV/c^2
Electron energy scale	ttop25	+1% shift	173.002±0.036	$\Delta M/2$ =	0.26
		-1% shift	172.491±0.036	0.255±0.026	
Muon energy scale	ttop25	+1% shift	172.974±0.036	$\Delta M/2$ =	0.26
		-1% shift	172.463±0.036	0.255±0.026	
Total lepton energy scale systematic error					**0.36**

Table 8: Systematics for the lepton energy scale.

6.4 Generators and radiation effects

The effect of the choice of a particular Monte Carlo generator is studied by comparing our default PYTHIA generator to HERWIG. These generators differ in the hadronization models, handling of the underlying $p\bar{p}$ events, and in the spin correlations in the production and decay of the $t\bar{t}$ pairs. The difference between masses obtained from the PE's sets performed with the two generators is found. This gives the systematic uncertainty due to the generator choice (see Table 9). As a cross-check we consider the results for Alpgen+Pythia and Alpgen+Herwig samples (Table 9). These generators differ only in the hadronization models.

Datasets	Mass, GeV/c^2	Mass Shift, GeV/c^2	Syst. GeV/c^2
ttop25 (Pythia)	172.72±0.17	ΔM=0.49±0.24	**0.49**
dtops0 (Herwig)	173.21±0.17		
dtopa2 (Alpgen+Pythia)	173.22±0.24	ΔM=-0.51±0.33	
dtopa3 (Alpgen+Herwig)	172.71±0.22		

Table 9: Generator systematics.

Also we estimate the systematic uncertainty due to the NLO effects by the comparison of the Pythia and Powheg+Pythia generators (see Table 10). The difference between masses obtained from the PE's sets performed with these two generators is taken as the estimation of systematic error due to NLO effects. As a cross-check, we consider the results from the Herwig and MC@NLO+Herwig samples (Table 10).

Datasets	Mass, GeV/c^2	Mass Shift, GeV/c^2	Syst. GeV/c^2
ttop25 (Pythia)	172.72±0.17	ΔM=-0.64±0.24	**0.64**
ttoppp (Powheg+Pythia)	172.08±0.17		
dtops0 (Herwig)	173.21±0.17	ΔM=0.72±0.3	
dtopn5 (MC@NLO+Herwig)	173.93±0.24		

Table 10: NLO systematics.

The effect of the initial and final state radiation (ISR and FSR) parametrization is studied, since jets radiated from interacting partons can be misidentified as leading jets and affect the top-quark mass measurement. The systematic uncertainty associated with ISR is obtained by adjusting the QCD parameters in the parton shower evolution in $t\bar{t}$ events. The size of this adjustment has been obtained from comparisons between Drell-Yan data and simulated events. Since the physics law that rule ISR and FSR is the same, the parameters that control ISR and

FSR are varied together (IFSR). Half of the difference in top-quark mass from PE's performed on samples with increased and decreased IFSR is taken as the systematic uncertainty for the ISR and FSR modeling (see Table 11).

Datasets	Mass, GeV/c^2	Mass Shift, GeV/c^2	Syst. GeV/c^2
ttop25 (nominal)	172.72±0.17		
dtops1 (more IFSR)	173.17±0.25	$\Delta M/2$=0.33±0.18	**0.33**
dtops2 (less IFSR)	172.51±0.25		

Table 11: IFSR systematics.

6.5 Color reconnection

The effect of color reconnection (CR) on our result is studied using the PYTHIA 6.4 MC generator, which includes CR effects. MC samples are generated using special tunes (ACRpro and Apro) with and without CR effects. We take the difference in the obtained masses from these MC samples as an estimation of systematic uncertainty due to the CR effects (see Table 12). As a cross check, we estimate effect of color reconnection using alternative tunes (Perugia0 and PerugiaNOCR). In both cases the mass shifts are consistent with zero within the uncertainties. So, we take the uncertainty of the mass shift (0.24 GeV/c^2) as our estimation of the CR systematic uncertainty.

Datasets	Mass, GeV/c^2	Mass Shift, GeV/c^2	Syst. GeV/c^2
ctopsd (tune Apro)	172.40±0.17	ΔM=0.14±0.24	
ctopse (tune ACRpro)	172.54±0.17		**0.24**
ctopsb (Perugia0)	172.19±0.17	ΔM=0.02±0.24	
ctopsc (PerugiaNOCR)	172.18±0.17		

Table 12: CR systematic uncertainty.

6.6 PDF's

The uncertainty in reconstructing the top quark mass due to the use of a particular parton distribution function (PDF) comes from three sources: PDF parametrization, PDF choice, and QCD scale (Λ_{QCD}). The recently developed next-to-leading order PDF from CTEQ6 allows

us to vary some PDF sets within their uncertainty. The possible variations are separated into contributions from 20 independent eigenvectors, so in total we have 41 different sets (1 nominal and 2×20 for $\pm 1\sigma$ variations). The PDF effect is studied using the reweighting method, where reconstructed top-mass templates for each PDF set are obtained from one single sample (Pythia *ttop25* 172.5 GeV/c^2 sample) by weighting each event by the probability for that event to proceed according to the given PDF. Results for the nominal PDF(CTEQ5L), alternative PDF's (MRST72, MRST75, CTEC6L, CTEQ6L1) and for the 20 pairs of $\pm 1\sigma$ CTEQ6M PDF are shown in Fig. 21. The black line corresponds to the nominal PDF set.

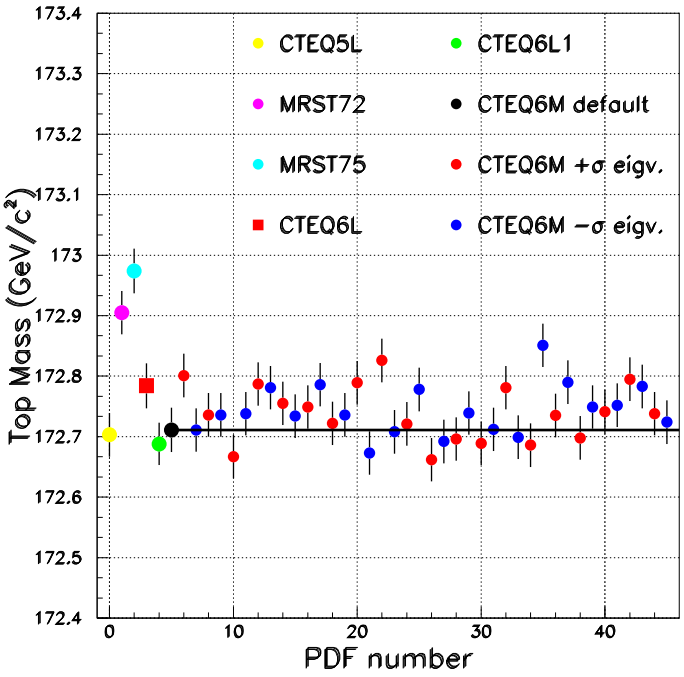

Figure 21: Results from PE's: output masses obtained on re-weighted *ttop25* sample and used to evaluate the PDF uncertainty. The results are presented for the nominal PDF(CTEQ5L), alternative PDF's (MRST72, MRST75, CTEC6L, CTEQ6L1) and for the 20 pairs of $\pm 1\sigma$ CTEQ6M PDF.

The uncertainty due to PDF parametrization is estimated by shifting by ±1 standard deviation one at a time the 20 eigenvectors of CTEQ6M. Half of the differences between the shifted masses derived from PE's are added in quadrature. The uncertainty due to the PDF choice is estimated as the difference between the top quark mass extracted by using CTEQ5L (default) and MRST72. The measured mass differences between MRST72, generated with $\Lambda_{QCD} = 300$ MeV, and MRST75, generated with $\Lambda_{QCD} = 228$ MeV, is taken as the uncertainty due to the choice of Λ_{QCD}. Results are summarized in Table 13.

Following the guidelines for evaluating the PDF systematics [11], we take the biggest value from the PDF systematic parametrization and the PDF choice. Obtained value (0.20 GeV/c^2)

is finally added in quadrature to Λ_{QCD} systematics (0.07 GeV/c^2) in order to get the total PDF systematic uncertainty, which is estimated to be 0.21 GeV/c^2.

Source	Uncertainty (GeV/c^2)
PDF parametrization	0.17±0.12
PDF choice	0.20±0.05
Λ_{QCD}	0.07±0.05
Total	**0.21**

Table 13: PDF systematic uncertainties on top quark mass.

6.7 Monte Carlo statistics

The effect of the limited statistics in the Monte Carlo samples is evaluated by the bootstrap method. We take the bias uncertainty (0.06 GeV/c^2) as value of systematics due to limited statistics of the signal MC samples (see Figure 17). Value of systematic error due to limited statistics of the background samples (0.18 GeV/c^2) is calculated as width of output mass distribution obtained from set of PE's performed on the bootstrapped background template. The total uncertainty due to the limited MC statistics is estimated as 0.19 GeV/c^2.

6.8 Pileup systematics

We consider two sources of uncertainty due to multiple $p\bar{p}$ interactions: the known and unknown mis-modelings. Known mis-modeling arises from the fact that the number of interactions in our Monte Carlo samples is not equal to the number observed in the data. Simulated events are tuned only to the first 2.8 fb^{-1} integrated luminosity of data. A possible discrepancy between simulated events and data collected at later times may affect the top-quark mass measurement. We evaluate this effect by running batches of PE's on $t\bar{t}$ events, selected according to the number of interaction vertices found in the event. The results from PE's are plotted against the number of interactions and fitted with a one degree polynomial (Fig. 22). The last point of this plot corresponds to events that have at least 4 interaction vertices. We use the slope (0.26 GeV/c^2/interaction) to derive the systematic uncertainty. We multiply 0.26 GeV/c^2/interaction by $< N_{vtx}^{data} > - < N_{vtx}^{MC} >$, where $< N_{vtx}^{data} >$=2.35 and $< N_{vtx}^{MC} >$=1.93 are the average number of vertices in the selected data sample and simulated sample respectively. We obtain a 0.11 GeV/c^2 uncertainty due to the known mis-modeling.

Unknown mis-modeling arises from fact that jet response versus number of vertices in Monte Carlo does not match what we would expect from the minimum bias data. According to the recipe from the Top Mass Group [11], we estimate the importance of this mis-modeling by scaling up the L4 systematics by a factor of 2.3·($< N_{vtx}^{data} >$-1)/($< N_{vtx}^{MC} >$-1). We obtain value of 0.30 GeV/c^2 for uncertainty due to the unknown mis-modeling. Finally, we take the larger of these two uncertainties (0.30 GeV/c^2) as systematic error due to pileup.

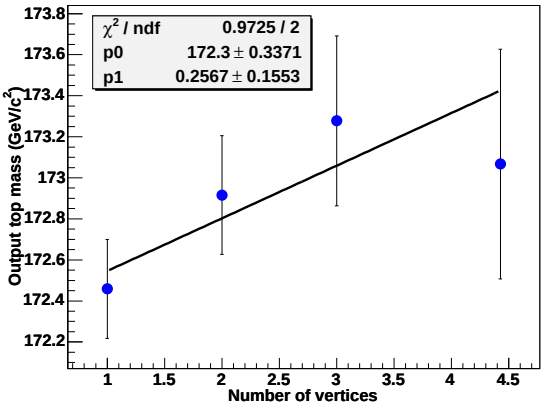

Figure 22: Results from PE's performed using events selected according to the number of interactions. The slope is indicated as P1.

6.9 gg fraction

Our nominal MC generator, Pythia, is a leading-order generator. So, number of $t\bar{t}$ events from gluon fusion in Pythia samples is approximately 6%. In case of the NLO framework, the gluon fusion fraction is expected to be 15%±5%. To estimate the uncertainty in the top mass due to this effect, we increase fraction of gg events by re-weighting of the nominal templates (see Table 14).

Datasets	Mass, GeV/c^2	Mass Shift, GeV/c^2	Syst. GeV/c^2
Pythia, ttop25; gg fraction 6%	172.72±0.04	ΔM=0.24±0.05	**0.24**
Reweighted ttop25; gg fraction 20%	172.96±0.04		

Table 14: gg fraction systematics.

6.10 b-tagging efficiency

A possible dependence of SF_{tag} (see Eq. 2) from jet E_T can be source of an uncertainty in our measurement. To check the sensitivity of our analysis to this effect, we introduce positive and negative slopes in SF_{tag} versus jet E_T dependence. Values of these slopes are defined by overall SF_{tag} uncertainty (±5%) and equal to ±0.00152. We obtain value of 0.05 GeV/c^2 for the uncertainty due to these effect (see Table 15).

Datasets	Mass, GeV/c^2	Mass Shift, GeV/c^2	Syst. GeV/c^2
ttop25; default SF_{tag}	172.72±0.04	$\Delta M/2$=0.05±0.05	**0.05**
ttop25; positive slope SF_{tag} from jet E_T	172.79±0.04		
ttop25; negative slope SF_{tag} from jet E_T	172.70±0.04		

Table 15: Calculation of the mass uncertainty due to the b-tagging efficiency uncertainty.

6.11 Background template shape

In order to estimate the systematic uncertainty for the background composition, diboson, Drell-Yan, and fakes expected rates are alternatively varied by plus or minus one standard deviation without changing the total number of expected background events. Half of the differences between $\pm$ 1 σ shifted masses derived from PE's are added in quadrature (Table 16).

In additon, the uncertainty on the shape of the fake background template is modeled. The fake rate E_T dependence is varied according to the fake rate uncertainties. Two shifted background templates are built and then used for PE's. The corresponding shift in mass is taken as the systematic uncertainty due to potential mis-modeling of fake shape. To estimate uncertainty on the shape of DY/Z background template we vary the relative fractions of 6 types of DY/Z background (see Section 3) inside their uncertainty intervals.

Source		Mass, GeV/c^2	Mass Shift, GeV/c^2	Syst., GeV/c^2
BG composition	Diboson(-σ)	172.75±0.04	$\Delta M/2$ =0.02±0.03	0.03
	Diboson(+σ)	172.71±0.04		
	DY(-σ)	172.51±0.04	$\Delta M/2$ =0.23±0.03	0.23
	DY(+σ)	172.96±0.04		
	Fakes(-σ)	173.02±0.04	$\Delta M/2$ =0.24±0.03	0.24
	Fakes(+σ)	172.53±0.04		
Fake shape	-linear E_T-dependent shift in fake rate matrix	172.75±0.04	$\Delta M/2$ =0.03±0.03	0.03
	+linear E_T-dependent shift in fake matrix	172.80±0.04		
Drell-Yan shape	variation of DY events amount in different kinematic regions	172.77±0.04	$\Delta M/2$ =0.04±0.03	0.04
		172.70±0.04		
Total				**0.33**

Table 16: Estimation of the background template shape uncertainty.

CDF Run II Preliminary (9.1 fb^{-1})

Source	Uncertainty (GeV/c^2)
Jet energy scale	2.42
NLO effects	0.64
Monte Carlo generators	0.49
Lepton energy scale	0.36
b-jet energy scale	0.34
Initial and final state radiation	0.33
Background modeling	0.33
Luminosity profile (pileup)	0.30
Color reconnection	0.24
gg fraction	0.24
Parton distribution functions	0.21
MC statistics	0.19
b-tagging	0.05
Total	**2.69**

Table 17: Summary of systematic uncertainties on the top quark measurement.

7 Results

The likelihood background constrained fit as described in Sec. 5 is performed on the dilepton data sample. Obtained results are presented in Table 18. The effective top-mass distributions from data for the b-tagged and non-tagged subsamples are shown in Figure 23. The mass-dependent negative log-likelihood function from the fit of the dilepton data sample is presented in Figure 24. Also post-fit plots for our initial variables, the reconstructed mass and M_t^{alt} are presented in Figures 25 and 26.

In order to check that the measured statistical error is reasonable, a set of PE's is performed on simulated background and signal events with $M_t = 171$ GeV/c^2 (close to the central value of the constrained fit). The obtained symmetrized error distribution along with the observed value (represented by the arrow) are shown in Figure 27. We estimate that the probability for obtaining a precision better then found in this experiment (p-value) is 68%. This value is obtained by comparing the measured uncertainties with those expected from PE's.

Parameter	Fit result
M_t	$\mathbf{170.80}\pm^{1.86}_{1.81}$ **(GeV/c^2)**
n_s^{tag}	$216.74\pm^{15.64}_{15.18}$
n_b^{tag}	$13.70\pm^{2.85}_{2.84}$
n_s^{notag}	$181.27\pm^{20.57}_{20.10}$
n_b^{notag}	$105.09\pm^{13.31}_{13.11}$

Table 18: Data fit results: values of top quark mass, numbers of signal and background events in b-tagged and non-tagged subsamples.

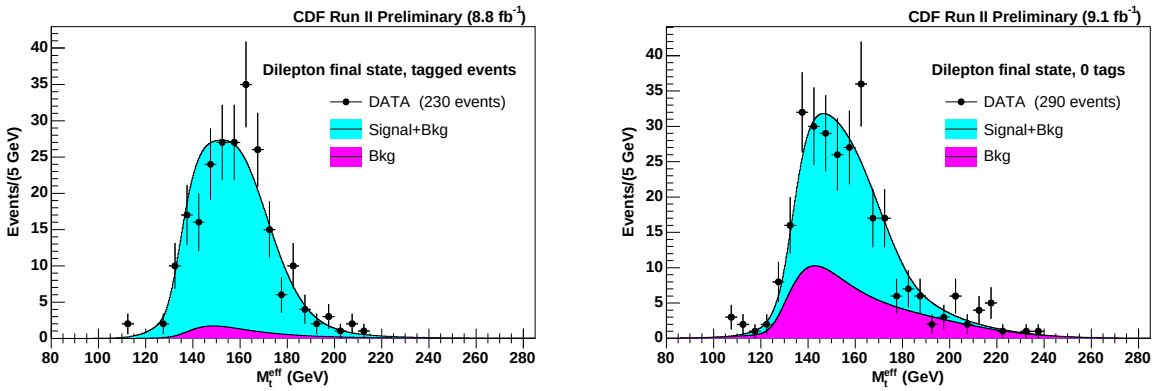

Figure 23: Likelihood fit to the dilepton data sample. The background (purple solid) and signal+background (cyan solid) p.d.f.'s, normalized according to the number of events returned by the fit, are superimposed to the effective top-mass distribution from data (histogram). Left and right plots show the b-tagged and non-tagged subsamples respectively.

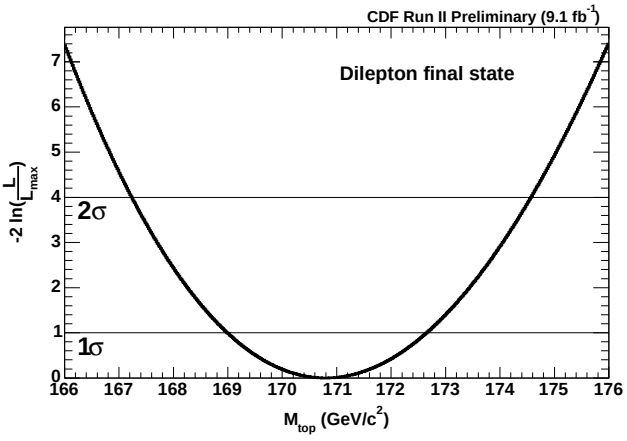

Figure 24: The mass-dependent negative log-likelihood function from the likelihood fit to the dilepton data sample.

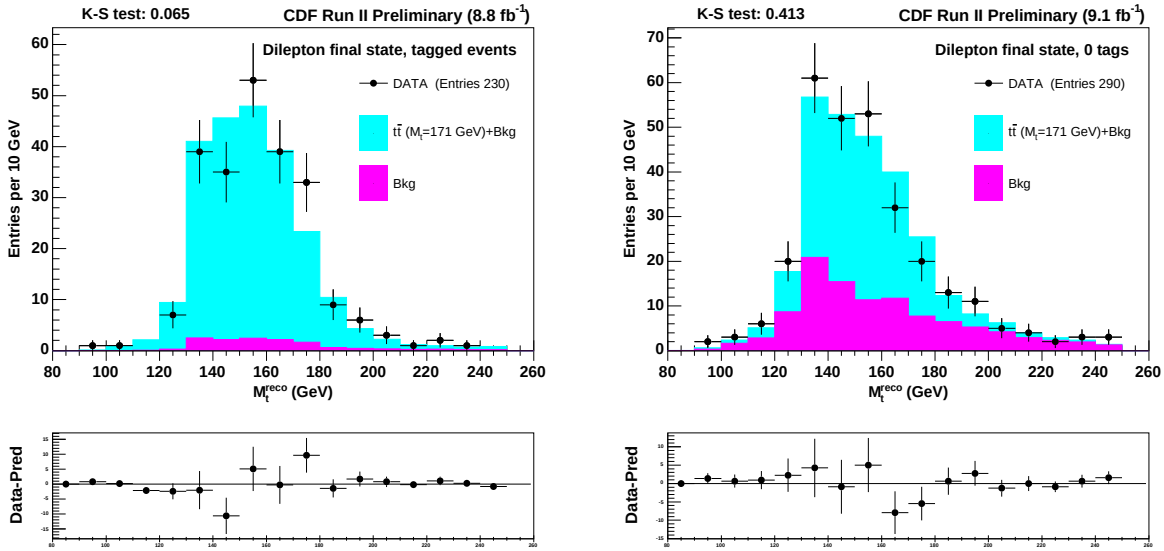

Figure 25: The background (purple solid) and signal+background (cyan solid) templates for the reconstructed top quark mass, normalized according to the number of events returned by the fit, are superimposed to the reconstructed mass distribution from data (histogram). Left and right plots show the b-tagged and non-tagged subsamples respectively. The input value of the top mass is 171 GeV/c^2 (close to the central value of the data fit).

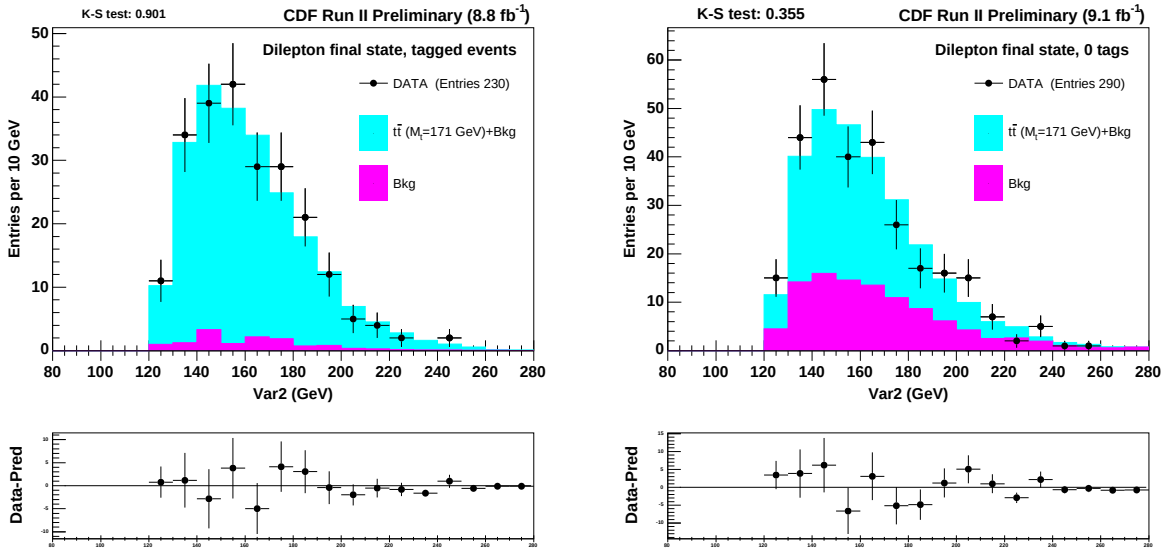

Figure 26: The background (purple solid) and signal+background (cyan solid) templates for the M_t^{alt} variable, normalized according to the number of events returned by the fit, are superimposed to the M_t^{alt} variable distribution from data (histogram). The left and right plots show the b-tagged and non-tagged subsamples respectively. The input value of the top mass is 171 GeV/c^2 (close to the central value of the data fit).

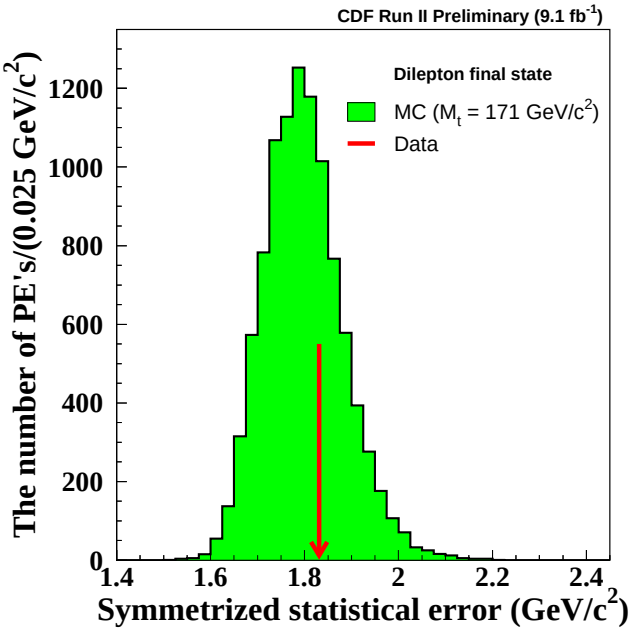

Figure 27: Symmetrized statistical errors from PE's generated with the top quark mass of 171 GeV/c^2. The arrow indicates the error obtained in this measurement.

8 Data Cross-checks

Different cross-checks of the result are performed using the data sample. We remove the background constraints from the likelihood function in order to check how the result may change. Also, we divide the data sample into different subsamples and measure the top mass on each subsample. Obtained results are presented in Table 19. We don not observe any differences in the cross-checks results which cannot be explained by a statistical fluctuation. The maximum deviation between two measurements (b-tagged and non-tagged samples) is 1.9σ.

9 Conclusions

Using the full Run II CDF data sample we measure the top-quark mass in the dilepton channel

$$\begin{aligned} M_{top} &= 170.80 \pm 1.83 \text{ (stat.)} \pm 2.69 \text{ (syst.) GeV}/c^2 \\ &\text{or} \\ M_{top} &= 170.80 \pm 3.25 \text{ GeV}/c^2 \end{aligned} \tag{26}$$

This result is compatible with the Tevatron average of the top-quark mass ($M_{top} = 173.20 \pm 0.87$ GeV/c^2 [1]), obtained by combining the CDF and DØ Run I and Run II results. Comparing with the last CDF result in this channel ($M_{top} = 170.28 \pm 3.69$ GeV/c^2 [2]) the improvement of about 10% in the total error has been achieved.

	M_t, (GeV/c^2)	n_s^{tag}	n_b^{tag}	n_s^{notag}	n_b^{notag}
Result	$\mathbf{170.80}\pm^{1.86}_{1.81}$	$216.74\pm^{15.64}_{15.18}$	$13.70\pm^{2.85}_{2.84}$	$181.27\pm^{20.57}_{20.10}$	$105.09\pm^{13.31}_{13.11}$
Bg. unconstrained fit	$171.27\pm^{1.88}_{1.81}$	$230.02\pm^{15.48}_{23.61}$	$0.00\pm^{20.67}_{0.00}$	$154.97\pm^{31.24}_{32.38}$	$135.03\pm^{29.93}_{33.01}$
b-tagged subsample	$173.10\pm^{2.31}_{2.23}$	$216.88\pm^{15.72}_{15.09}$	$13.63\pm^{2.84}_{2.85}$	-	-
Non-tagged subsample	$165.58\pm^{3.23}_{3.16}$	-	-	$180.58\pm^{19.87}_{20.40}$	$105.55\pm^{13.15}_{12.98}$
$\leq$p17, bg. unconstr. fit	$171.09\pm^{3.39}_{3.20}$	$71.13\pm^{8.63}_{17.60}$	$0.00\pm^{16.69}_{0.00}$	$48.56\pm^{16.86}_{18.87}$	$44.50\pm^{19.64}_{15.82}$
p18-p25, bg. unconstr. fit	$175.63\pm^{3.64}_{3.52}$	$59.06\pm^{7.97}_{12.88}$	$0.00\pm^{11.83}_{0.00}$	$46.12\pm^{12.77}_{14.58}$	$18.02\pm^{14.43}_{10.74}$
p26-p33, bg. unconstr. fit	$167.11\pm^{3.34}_{3.17}$	$64.12\pm^{8.22}_{16.94}$	$0.00\pm^{16.06}_{0.00}$	$43.90\pm^{16.10}_{18.13}$	$44.15\pm^{19.01}_{15.20}$
p34-p38, bg. unconstr. fit	$173.27\pm^{6.81}_{5.44}$	$36.07\pm^{6.27}_{8.85}$	$0.00\pm^{7.98}_{0.00}$	$17.78\pm^{14.08}_{14.75}$	$27.36\pm^{19.45}_{13.56}$

Table 19: Cross-checks on the data.

References

[1] Combination of CDF and DØ results on the mass of the top quark using up to 8.7 fb^{-1} of $p\bar{p}$ collisions. *CDF Note 10976, DØ Note 6381*, 2013

[2] Hyun-Su Lee et al, Top quark mass measurement in the Lepton+Jets and Dilepton Cannels using 5.6 fb^{-1} data. *CDF Note 10268*, 2010

[3] Measurement of the top quark mass in $p\bar{p}$ collisions using events with two leptons. *DØ Collaboration*; Phys. Rev. D 86, 051103(R) (2012), arXiv:1201.5172

[4] Chang-Seong Moon et al, Measurement of Top Dilepton Cross Section with CDF Full data using the DIL Selection. *CDF Note 10877*, 2013

[5] http://www-cdf.fnal.gov/internal/physics/top/RunIIMC/topmc6/index.shtml

[6] L. Lyons, D. Gibaut, and P. Clifford, Nucl. Instrum. Meth. A270 (1988) 110;
A. Valassi, Nucl. Instrum. Meth. A500 (2003) 391

[7] Measurement of the Top Quark Mass at CDF using the "neutrino phi weighting" Template Method on a Lepton Plus Isolated Track Sample, T. Aaltonen et al., *The CDF Collaboration*, Phys. Rev. D79, 072005 (2009), arXiv: 0901.3773

[8] A. Abulencia *et al.* (CDF Collaboration), Phys. Rev. D 73, 032003 (2006).

[9] M. Beneke *et al.*, Top Quark Physics, arXiv:hep-ph/0003033.

[10] F. James, *MINUIT: Function Minimization and Error Analysis*, CERN Program Library, D506.

[11] http://www-cdf.fnal.gov/internal/physics/top/run2mass/systematics_08_add.html;
http://www-cdf.fnal.gov/internal/physics/top/run2mass/systematics_08.html